Journal of Physics A:
Mathematical and
Theoretical

PURPOSE-LED
PUBLISHING™

PAPER • **OPEN ACCESS**

Measured dynamics of an XXZ quantum simulator in a highly symmetrical double-ringed geometry

To cite this article: D J Papoular 2026 *J. Phys. A: Math. Theor.* **59** 415301

View the article online for updates and enhancements.

You may also like

- Fifth Symposium on Prospects in the Physics of Discrete Symmetries
- Lie symmetry analysis of the two-Higgs-doublet model field equations
M Aa Solberg
- The 5th International Symposium in Quantum Theory and Symmetries (QTS5)
O Arratia, J A Calzada, F Gómez-Cubillo et al.

This content was downloaded from IP address 86.242.140.82 on 16/11/2026 at 18:11

Journal of Physics A: Mathematical and Theoretical

Check for updates

PAPER

OPEN ACCESS

RECEIVED
28 June 2026

REVISED
8 September 2026

ACCEPTED FOR PUBLICATION
30 September 2026

PUBLISHED
13 October 2026

Original content from this work may be used under the terms of the Creative Commons Attribution 4.0 licence.

Any further distribution of this work must maintain attribution to the author(s) and the title of the work, journal citation and DOI.

Measured dynamics of an XXZ quantum simulator in a highly symmetrical double-ringed geometry

D J Papoular*

Laboratoire de Physique Théorique et Modélisation, UMR 8089 CNRS & CY Cergy Paris Université, 95302 Cergy–Pontoise, France

* Author to whom any correspondence should be addressed.

E-mail: david.papoular@cyu.fr

Keywords: trapped rydberg atoms, discrete symmetries, Heisenberg and XXZ models

Abstract

We theoretically identify observable consequences of spatial and spin symmetries on the dynamics of a small XXZ quantum simulator. Our proposed protocol relies on the choice of suitable initial states, and involves the measurement scheme whose experimental implementation is the simplest. We analyze a system of $N = 2n = 6$ to 12 particles, trapped in a planar geometry comprised of two rings which exhibits point group symmetry D_{nh}. The particles represent effective spins whose interaction is described by the XXZ or Heisenberg Hamiltonian. The system is prepared in an initial state which is sitewise-factorized and invariant under all spatial symmetries, it evolves for a given time, after which the z-components of all N spins are measured. We show that symmetries dictate (*i*) the qualitative behavior of the measurement probabilities as a function of the evolution time, and (*ii*) the number of measurement results with different probabilities. We highlight the role of a twofold rotation of all spins. We also demonstrate that, in larger systems, the collapse of the initial state may be observed.

1. Introduction

The symmetries of a system provide a wealth of information concerning it without the need for an explicit solution. In the context of quantum mechanics, they have been exploited to explain the degeneracies of the energy spectrum, to analyze energy level splittings due to perturbations, and to establish selection rules [1, chapter 1]. They have been instrumental in the interpretation of the energy spectra of atoms, molecules, and crystals [2, chapters 6–8]. Their impact on quantum dynamics has long been investigated (see e.g. [3, section 11.5]).

There is a fundamental interest in studying spin systems whose sites exhibit high spatial symmetry. These systems exhibit two types of symmetries: firstly, the discrete symmetries affecting the positions of the particles, and secondly, the continuous or discrete symmetries affecting their spins. Symmetries of one type may be applied to the system independently of those of the other. The set of all symmetries, comprised of symmetries of both types and of their products, is a spin point group [4, 5]. Such symmetry groups are currently being investigated in the context of condensed matter physics [6, 7]

These highly-symmetrical spin systems may be realized, manipulated, and measured, owing to recent experimental progress in the field of quantum simulation [8, 9]. There, conceptually simple systems are constructed using N trapped particles which may be e.g. magnetic atoms, alkali atoms in Rydberg states, or polar molecules [10, 11], including the minimal ingredients yielding the sought effect. The particles may be confined in well-controlled individual traps arranged in arbitrary geometries [11–16]. Each particle represents a two-level system. The system may be prepared in an initial N-particle state which is an arbitrary tensor product of individual spin states by applying local electromagnetic pulses [17, section 1.5.2]. The pair-wise interaction between the particles may be tailored to simulate a spin system described by the Heisenberg or XXZ Hamiltonians [18–21]. The system evolves under this Hamiltonian for a given time. Then, the final state of the N particles may be measured using optical methods [12, 13,

© 2026 The Author(s). Published by IOP Publishing Ltd

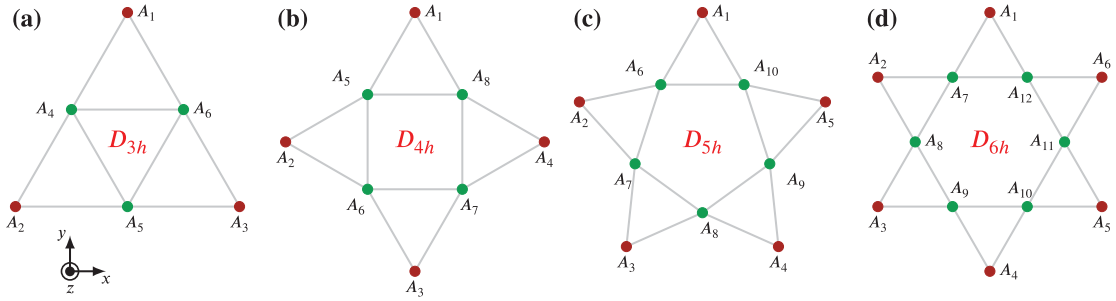


Figure 1. The four considered geometries, each comprised of an even number $N = 2n$ of particles with $n = 3$ (a), 4 (b), 5 (c), and 6 (d), trapped in the (x, y) plane at the sites $(A_i)_{1\leqslant i\leqslant N}$, with one particle per site. Each geometry exhibits point group symmetry D_{nh}, but no translational invariance. It involves a double-ring structure, with n particles on the outer ring (sites $1\leqslant i\leqslant n$, shown in red) and n particles on the inner ring (sites $n+1\leqslant i\leqslant N$, shown in green). Neighboring atoms linked by gray segments are equidistant.

22, 23]. Multiple realizations of the experiment provide the measurement probabilities. Such schemes have already allowed for the experimental characterization of e.g. 2D antiferromagnets [14, 24].

Observable signatures of the high symmetry of the Hamiltonian of a quantum system are subtle to identify. This is due to the fact that observed signals result from two consecutive steps: the quantum evolution, followed by a quantum measurement. The evolution is piloted by the Hamiltonian and, hence, enforces the conservation laws corresponding to all its symmetries. The measurement of a given observable is characterized by a specific basis of the N-particle Hilbert space, comprised of its eigenstates, which are the possible measurement results [25, section VIII-2]. For the measurement to enforce the conservation laws of the Hamiltonian, this basis should be comprised of symmetry-adapted linear combinations [26, chapter 6], i.e. states each transforming under an irreducible representation of the symmetry group [27, § 94]. However, the measurement of arbitrary observables is currently out of experimental reach [17, section 4.5.4]. The accessible observables are determined by experimental requirements, and their eigenstates are not adapted to the larger symmetry groups. Thus, the probability amplitudes characterizing the measurement result from the interference between components of the wavefunction with different symmetry properties. This interference is similar to that which affects the measurement of a dressed two-level system, yielding Rabi oscillations in the probability amplitudes as a function of time [28, section IV.C.3]. If the interference is not avoided, the measurement probabilities exhibit no clear signature of the symmetries of the Hamiltonian. One way of avoiding it, already considered in the literature (see e.g. [29, 30]), is to measure well-chosen observables compatible with a specific subset of operations in the symmetry group.

In this article, we propose an alternative approach applicable to spin systems with high spatial symmetry. We show that the interference may be avoided by selecting suitable initial states, all easily prepared, which are invariant under all spatial symmetries. Their quantum evolution may be probed by the measurement scheme whose experimental implementation is the most straightforward, namely, the simultaneous measurement of the z-components of all spins. We identify signatures of the spatial and spin symmetries of the Hamiltonian in the time dependence of the resulting measurement probabilities.

We present our approach on the case of a system of effective spins represented by particles which may be either bosonic or fermionic, confined in a planar geometry. In order for our analysis to be relevant to current experiments, we keep their number N relatively small, and consider up to a dozen particles. Two-dimensional systems comprised of so few particles would realize only a poor approximation of lattice translational invariance. Therefore, we do not seek to simulate a crystal, but rather a highly symmetrical molecule. Thus, the spatial symmetries of the considered systems make up a point group [27, § 93], specifically D_{nh} with $n = 3$, 4, 5, or 6 and $N = 2n$. The considered geometries, represented in figure 1, are each comprised of two concentric rings involving n particles. Compared to geometries involving a single ring, the double-ring structure allows for a greater variety of experimentally accessible initial states, a flexibility we shall explicitly use.

The dynamics of the N-particle system we are considering is governed either by the Heisenberg Hamiltonian, or by the more general XXZ Hamiltonian. Our choice of initial states constrains the quantum dynamics of the N-particle system to occur within the subspace of the full Hilbert space comprised of the states which are invariant under all spatial symmetries. The dimension of this subspace plays a

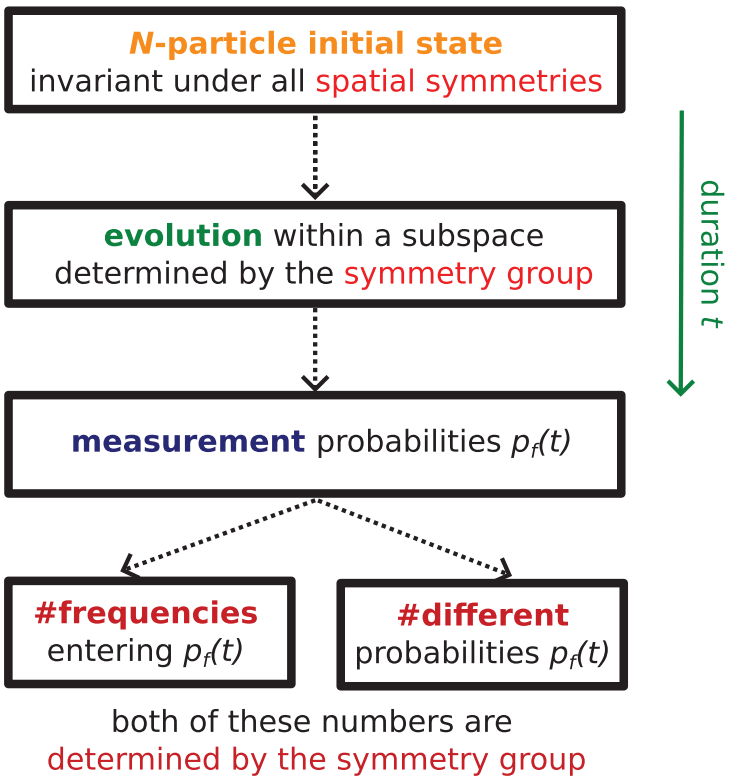


Figure 2. Schematics of the main physical mechanism.

key role, and we show that its value has two observable consequences on the measurement probabilities. Firstly, this dimension determines the qualitative behavior of the probabilities as a function of the evolution time: these may be constant, or oscillate sinusoidally, or undergo an aperiodic evolution. Secondly, symmetries cause many of the possible measurement results to have the same probability at all times, and the number of possible measurement results with different probabilities is equal to the dimension of the subspace within which the evolution occurs.

In the specific case of the XXZ Hamiltonian, we analyze the role of the twofold rotations of the N spins about an axis in the horizontal plane (plane of figure 1), and explain how the conservation of the corresponding parity may be stringently tested on smaller systems, comprised of $N = 6$ spins.

Finally, we identify an effect occurring in larger systems comprised of e.g. $N = 12$ spins, namely, the collapse of the component of the initial state with zero total spin projection. Here, in accordance with the literature on the Jaynes–Cummings model [31, 32] and other atomic physics experiments (see e.g. [33]), we use the term 'collapse' to refer to the following process, described by the Schrödinger equation: The dephasing between many terms, entering the time evolution of the wavefunction and oscillating with incommensurate frequencies, causes the initially maximal population of a single configuration to redistribute over many inequivalent configurations, such that no individual outcome retains a large probability.

Experimental accessibility of the considered geometries — The geometries of figure 1 may be realized e.g. by trapping the individual particles in 2D arrays of optical tweezers, which may have arbitrary geometries [34]. For example, the geometry of figure 1d is a finite-sized fraction of the Kagome lattice realized for the experiment of [16] involving trapped interacting Rydberg atoms.

Presentation of the central physical mechanism

The main physical mechanism analyzed in this paper is shown schematically in figure 2. We briefly summarize it here before presenting the details in the rest of the paper.

The system of $N = 2n$ effective spins is described using a Hamiltonian exhibiting high spatial symmetry. We choose a suitable N-particle initial state, let it evolve for a given duration t, and then measure the z-component of each of the N spins, yielding 2^N measurement probabilities $p_f(t)$. This measurement is unrelated to the spatial symmetry group, hence, for an arbitrary initial state, the measurement probabilities exhibit no straightforward consequences of spatial symmetry.

We choose an initial N-particle state which is invariant under all spatial symmetries. This constrains the quantum evolution up to time t, just before the measurement is performed, to occur within the subspace of Hilbert space comprised of the N-particle states satisfying the same property. We show in section 4 that this constraint restricts both (A) the number of frequencies entering the probabilities $p_f(t)$ and (B) the number of different functions $p_f(t)$. Both of these numbers are determined by the dimension of the subspace within which the evolution occurs.

Importance of the dimension of the subspace (ρ_1, M) — More specifically, the essential subspace to consider is the subspace (ρ_1, M) comprised of all N-particle states which are (i) invariant under all spatial symmetries, and (ii) eigenstates of the total spin projection operator S_z with eigenvalue $\hbar M$. This subspace is fully determined by the symmetry group of the N-particle system, i.e. it does not depend on the parameters entering the spin Hamiltonian [27, § 94]. Under the assumption on the initial state stated above, the dimension $d = \dim(\rho_1, M)$ has two physical interpretations:

(A) Considering the quantum evolution, symmetry constrains the wavefunction component with total spin projection M to evolve within the subspace (ρ_1, M). Hence, its time dependence involves d frequencies, and that of the corresponding measurement probabilities involves $d(d-1)/2$ transition frequencies (see section 4.1).

(B) Considering the measurement results, d is the number of results which are inequivalent, i.e. which do not correspond to each other through a spatial symmetry. This is the number of measurement results with different probabilities (see section 4.2).

The dimension d is usually calculated using well established group-theoretical methods [27, § 94]. The property (B) above shows that our proposed experiment provides a way of measuring d experimentally, by counting the number of measurement results with different probabilities.

Outline

This article is organized as follows. In section 2, we introduce the considered N-particle system and its Hamiltonian, and put forward our proposed protocol. In section 3, we describe the spatial and spin symmetries of the system, and select initial states allowing for their investigation. In section 4, we identify two observable consequences of symmetry on the time dependence of the measurement probabilities: their qualitative behavior, and the number of measurement results with different probabilities. In section 5.1, we analyze specific cases within experimental reach. We highlight the role of the twofold rotation of the N spins, which may be probed on smaller systems ($N = 6$) described by the XXZ Hamiltonian. We also demonstrate that larger systems ($N = 12$) allow for the observation of the collapse of the initial state. Finally, we conclude in section 6.

2. Considered system and protocol

2.1. System and effective spin Hamiltonian

We consider the four geometries of figures 1(a)–(d), respectively comprised of $N = 2n = 6$, 8, 10, and 12 particles trapped at the sites $(A_i)_{1\leqslant i\leqslant N}$ whose positions are $(\boldsymbol{r}_i)_{1\leqslant i\leqslant N}$, with one particle per site. These geometries are planar, with all sites lying in the (xy) plane. They consist of two rings, each comprised of n sites. The sites on the outer ($1\leqslant i\leqslant n$) and inner ($n+1\leqslant i\leqslant N$) rings appear in red and green, respectively, in figure 1. The neighboring sites linked by gray segments are equidistant.

We neglect the spatial motion of the particles within the traps. Each particle i behaves as a two-level system, whose two accessible quantum states we call $|\uparrow_i^z\rangle$ and $|\downarrow_i^z\rangle$. The particles exhibit pairwise interaction, whose strength depends on the distance $r_{ij} = |\boldsymbol{r}_j - \boldsymbol{r}_i|$ between the sites A_i and A_j through the power law $1/r_{ij}^\alpha$ with $\alpha > 0$, with $\boldsymbol{r}_i$ being the position of the site A_i. The N-particle Hamiltonian H involves interactions between all pairs of particles but no intersite tunneling:

$$H = \frac{1}{2}\sum_{i\neq j}\left(\frac{a}{r_{ij}}\right)^\alpha \left[J(\sigma_i^x\sigma_j^x + \sigma_i^y\sigma_j^y) + J_z\sigma_i^z\sigma_j^z\right] , \tag{1}$$

where a is the nearest-neighbor distance ($a = r_{14}$, r_{15}, r_{16}, and r_{17}, respectively, for the four geometries of figure 1). The Pauli operators $\boldsymbol{\sigma}_i = (\sigma_i^x, \sigma_i^y, \sigma_i^z)$ represent the two-level system trapped at A_i. The coefficients J and J_z are constant energies. The Hamiltonian H is the Heisenberg Hamiltonian H_{H} or the XXZ Hamiltonian H_{XXZ} depending on whether $J = J_z$ or $J \neq J_z$. It has already been used in the literature to describe assemblies of interacting Rydberg atoms (see e.g. [20, 21]).

Regardless of the bosonic or fermionic nature of the actual trapped particles, the simultaneous assumptions of a single particle per site and no intersite tunneling allow us to describe the system in terms of N distinguishable effective spins–1/2, represented by the operators $\boldsymbol{s}_i = \hbar\boldsymbol{\sigma}_i/2$.

Choice of the parameters entering the Hamiltonian of equation (1) — We have performed all the numerical calculations reported in this paper using $\alpha = 6$, $J > 0$, and $-3 < J_z/J < 3$, matching the proposal[1] of [21] involving circular Rydberg atoms. However, these choices are not critical, and our analysis may be extended to other experimental realizations of the 2D Heisenberg and XXZ models (with magnetic atoms, Rydberg atoms, or polar molecules, see e.g. [10, 20, 22]).

2.2. Protocol yielding time-dependent probabilities

We analyze the following protocol ($\mathcal{P}$). The system is initially prepared in an N-particle state $|\psi_0\rangle$. It evolves under the Hamiltonian H of equation (1) for the duration t, giving rise to the quantum state $|\psi(t)\rangle = \mathrm{e}^{-\mathrm{i}Ht/\hbar}|\psi_0\rangle$. At time t, we measure the observable s_i^z for each of the N spins. This yields one of 2^N possible results, namely, the N-particle state $|c_f\rangle = |\mu_1, \ldots, \mu_N\rangle$ where the spin at site A_i is in the state $|\mu_i\rangle = |\uparrow_i^z\rangle$ or $|\downarrow_i^z\rangle$. The 2^N configurations $|c_f\rangle$ make up the basis $\mathcal{C} = (|c_f\rangle)_{1\leqslant f\leqslant 2^N}$ of the full Hilbert space $\mathcal{H}$. (The ordering of the basis states $|c_f\rangle$ is detailed in appendix A).

Such a measurement is experimentally accessible (see [23] for a recent demonstration with circular Rydberg atoms). Multiple repetitions of the sequence, with the same initial state $|\psi_0\rangle$ and duration t, give access to the probabilities $p_f(t) = |\langle c_f|\psi(t)\rangle|^2$ for the measurement to yield the result $|c_f\rangle$. These probabilities depend on the chosen time t.

The goal of the present work is to identify experimentally accessible properties of the time-dependent $p_f(t)$'s, holding for specific initial states $|\psi_0\rangle$, which exhibit signatures of the spatial and spin symmetries of the N-particle system.

3. Symmetries of the Hamiltonian and choice of the initial states

3.1. Spin-point group comprising spatial and spin symmetries

We present the group of all symmetries of the Hamiltonian H represented by unitary operators as a spin-point group [4, 5] $G = G^{\mathrm{spatial}} \times G^{\mathrm{spin}}$, which is the direct product of the group G^{spatial} acting on the positions while leaving the internal states of the effective spins unchanged, and the group G^{spin} acting on the internal states while leaving the positions unchanged.

Spatial symmetries — The trapping geometries of figure 1, involving at most 12 sites, do not exhibit translational invariance. Accordingly, their spatial symmetry properties are those of a molecule (rather than of a crystal). The spatial symmetry group of the geometry involving $N = 2n$ particles is the point group $G^{\mathrm{spatial}} = D_{nh}$ [27, § 93]. It contains $4n$ elements, all obtained as products of the rotation of order n about the axis $\boldsymbol{z}$, the rotation of order 2 about the axis $\boldsymbol{y}$, and the reflection in the horizontal plane (Oxy). Each element of D_{nh} is characterized by a permutation ϕ mapping the N sites $(A_i)_{1\leqslant i\leqslant N}$ onto $(A_{\phi(i)})_{1\leqslant i\leqslant N}$. Then, the unitary operator U_ϕ representing this element, which acts on the Hilbert space $\mathcal{H}$, maps each configuration $|c_f\rangle = |\mu_1, \ldots, \mu_N\rangle$ in the basis $\mathcal{C}$ onto the configuration $U_\phi|c_f\rangle = |\mu_{\phi^{-1}(1)}, \ldots, \mu_{\phi^{-1}(N)}\rangle$, also in $\mathcal{C}$.

Spin symmetries — The spin symmetry group G^{spin} depends on the values of J and J_z in equation (1). If $J = J_z$ (i.e. $H = H_{\mathrm{H}}$), $G^{\mathrm{spin}} = K_h$ is the group of complete spherical symmetry [27, § 98], including spin rotations through any angle about any axis in three-dimensional space. If $J \neq J_z$ (i.e. $H = H_{\mathrm{XXZ}}$), G^{spin} is the smaller group $D_{\infty h}$, including spin rotations through any angle about the z axis, and spin rotations through angle π about any horizontal axis. In both cases, each element g in G^{spin} is represented by the unitary operator $U_g = u_g^{(1)} \cdots u_g^{(N)}$, where $u_g^{(i)}$ acts on the state of the spin at site A_i in the same way as it would act on a true spin-1/2 [35, sections XIII.19 & XV.10].

3.2. Interplay between conservation laws and measurement

The symmetries of section 3.1 yield conservation laws which hold at all times during the evolution described by the Schrödinger equation, i.e. up to just before the measurement is performed. We point out two of them which are valid for both the Heisenberg and the XXZ Hamiltonians. Firstly, the presence in G^{spin} of all rotations about the axis $\boldsymbol{z}$ yields the conservation of the total spin projection operator

[1] In the proposal of [21], the single-atom states $|\uparrow_i\rangle$ and $|\downarrow_i\rangle$ are respectively encoded into circular Rydberg states with principal quantum numbers $n = 50$ and 48, and the distance between nearest-neighboring atoms is $a \approx 5\,\mu$m. Hence, the interatomic distance greatly exceeds the spatial extent $n^2 a_0 \sim 0.1\,\mu$m of the single-atom wavefunctions. Then, equation (1) is applicable with $\alpha = 6$, $J/h = 17\,$kHz, and $-3 < J_z/J < 3$ (see [21, section II and App. A]).

$S_z = \sum_{i=1}^{N} s_i^z$ [27, § 26]. Secondly, if the initial N-particle state $|\psi_0\rangle$ transforms according to a given irreducible representation ρ of the spatial symmetry group D_{nh}, then so does the N-particle state $|\psi(t)\rangle$ [27, § 97]. Any initial state $|\psi_0\rangle$ is a linear superposition of components $|\psi_0^{\rho,M}\rangle$, each of which transforms according to the irreducible representation ρ of D_{nh} and is an eigenstate of S_z with eigenvalue $\hbar M$, where the total spin projection M is an integer such that $-n \leqslant M \leqslant n$. Owing to the two conservation laws stated above, these components evolve independently from one another up to just before the measurement, and $|\psi(t)\rangle = \sum_{\rho,M} |\psi^{\rho,M}(t)\rangle$ with $|\psi^{\rho,M}(t)\rangle = \mathrm{e}^{-\mathrm{i}Ht/\hbar}|\psi_0^{\rho,M}\rangle$.

We now discuss the impact of these two conservation laws on the probability amplitude $\langle c_f|\psi(t)\rangle$ for the measurement performed at time t to yield the result $|c_f\rangle = |\mu_1, \ldots, \mu_N\rangle$, which is an N-particle state in the basis $\mathcal{C}$. Firstly, we consider the total spin projection. The state $|c_f\rangle = |c_f^{M_f}\rangle$ is an eigenstate of the operator S_z with the eigenvalue $\hbar M_f$, where the total spin projection $M_f = \sum_{i=1}^{N} \mu_i$ and $\mu_i = \pm 1/2$ according to whether $|\mu_i\rangle = |\uparrow_i^z\rangle$ or $|\downarrow_i^z\rangle$. Therefore, only the components $|\psi^{\rho,M_f}(t)\rangle$ with $M = M_f$ contribute to $\langle c_f|\psi(t)\rangle$.

Secondly, we turn to the irreducible representations ρ of the spatial symmetry group D_{nh}. Most states $|c_f\rangle$ in the basis $\mathcal{C}$ do not transform under a specific irreducible representation ρ. Instead, they are superpositions $|c_f\rangle = \sum_\rho |c_f^\rho\rangle$ of multiple components $|c_f^\rho\rangle$, each transforming under a given representation ρ. Then, the probability amplitude $\langle c_f|\psi(t)\rangle$ reads:

$$\langle c_f|\psi(t)\rangle = \sum_\rho \langle c_f^\rho|\psi^{\rho,M_f}(t)\rangle \ . \tag{2}$$

Unless the sum in equation (2) reduces to a single term, the measurement causes interference between the wavefunction components $|\psi^{\rho,M_f}(t)\rangle$ with the same total spin projection M_f, but transforming under different irreducible representations ρ of D_{nh}, so that the probabilities $p_f(t) = |\langle c_f|\psi(t)\rangle|^2$ exhibit no clear signature of the spatial symmetry group D_{nh}.

3.3. The considered initial states

We avoid the interference identified in section 3.2 by selecting initial N-particle states $|\psi_0\rangle$ which transform under a given irreducible representation ρ_0 of the spatial symmetry group D_{nh}. Then, each component $|\psi^M(t)\rangle = |\psi^{\rho_0,M}(t)\rangle$ of $|\psi(t)\rangle$ with total spin projection M also transforms under ρ_0, and the sum of equation (2) reduces to a single term, $\langle c_f|\psi(t)\rangle = \langle c_f^{\rho_0}|\psi^{\rho_0,M_f}(t)\rangle$. In this equality, the representation ρ_0 is the one under which the initial state $|\psi_0\rangle$ transforms, whereas the total spin projection M_f is that of the measurement result $|c_f\rangle$.

This situation may be achieved experimentally by selecting initial states of the form $|\psi_0\rangle = |\chi_{\boldsymbol{u},\boldsymbol{v}}\rangle$ defined as follows:

$$|\chi_{\boldsymbol{u},\boldsymbol{v}}\rangle = |\uparrow_1^{\boldsymbol{u}}, \ldots, \uparrow_n^{\boldsymbol{u}}, \uparrow_{n+1}^{\boldsymbol{v}}, \ldots, \uparrow_N^{\boldsymbol{v}}\rangle \ , \tag{3}$$

where all n spins on the sites A_i of the outer ring ($i = 1$ to n) are in the same single-particle state $|\uparrow_i^{\boldsymbol{u}}\rangle$, and all n spins on the sites of the inner ring ($i = n+1$ to N) are in the same state $|\uparrow_i^{\boldsymbol{v}}\rangle$. The real unit vectors $\boldsymbol{u}$ and $\boldsymbol{v}$ represent two directions on the Bloch sphere [17, section 1.2], and for $\boldsymbol{w} = \boldsymbol{u}$ or $\boldsymbol{v}$, the state $|\uparrow_i^{\boldsymbol{w}}\rangle = \cos(\theta/2)\mathrm{e}^{-\mathrm{i}\phi/2}|\uparrow_i^z\rangle + \sin(\theta/2)\mathrm{e}^{\mathrm{i}\phi/2}|\downarrow_i^z\rangle$, with (θ, ϕ) being the spherical coordinates of $\boldsymbol{w}$.

The N-particle state $|\chi_{\boldsymbol{u},\boldsymbol{v}}\rangle$ is a tensor product of N single-particle states, hence, it may be prepared experimentally, e.g. starting from the polarized state $|\uparrow_1^z, \ldots, \uparrow_N^z\rangle$ and applying electromagnetic pulses to the individual spins [17, section 1.5.2].

The spatial symmetries in the group D_{nh}, acting on Hilbert space as the operators U_ϕ of section 3.1, permute the states of the n spins on the sites of the outer ring among themselves, and those of the n spins on the inner ring among themselves. Therefore, the state $|\chi_{\boldsymbol{u},\boldsymbol{v}}\rangle$ is invariant under all spatial symmetries. This amounts to stating that it transforms under the unit representation ρ_1 of D_{nh}, which is irreducible [27, § 94].

To sum up, the N-particle states $|\chi_{\boldsymbol{u},\boldsymbol{v}}\rangle$ of equation (3), which are experimentally accessible, transform under the unit representation ρ_1 of the spatial symmetry group D_{nh}. Their being indexed by two independent directions $\boldsymbol{u}$ and $\boldsymbol{v}$ follows from the presence of two rings in the geometries of figure 1. This family of states is sufficiently large to allow for the observation of various qualitative behaviors, discussed below, for the time dependence of the measurement probabilities.

States with maximal total spin modulus — As a special case of equation (3), we first consider the state $|\xi_{\boldsymbol{u}}\rangle = |\chi_{\boldsymbol{u},\boldsymbol{u}}\rangle = |\uparrow_1^{\boldsymbol{u}}, \ldots, \uparrow_N^{\boldsymbol{u}}\rangle$, describing $N = 2n$ particles all in the same single-particle state $|\uparrow_i^{\boldsymbol{u}}\rangle$, for a given direction $\boldsymbol{u}$ on the Bloch sphere with spherical coordinates (θ, ϕ). The state $|\xi_{\boldsymbol{u}}\rangle$ is an eigenstate of the squared total spin operator $\boldsymbol{S}^2 = (\boldsymbol{s}_1 + \ldots + \boldsymbol{s}_N)^2$ with the eigenvalue $\hbar^2 S(S+1)$, the total spin

Table 1. Dimensions of the subspaces (ρ_1, M) defined in section 4, with ρ_1 being the unit representation of D^{spatial}_{nh}, for the four geometries of figure 1. For $M = 0$, the states transforming under ρ_1 are further sorted in terms of their even or odd parity with respect to the operator Y^{spin}, representing the rotation of all spins through angle π about the axis $\boldsymbol{y}$. The non-applicable cells with $|M| > n$ are labeled 'N/A'.

	$N = 6$	$N = 8$	$N = 10$	$N = 12$
$(\rho_1, M = \pm 6)$	N/A	N/A	N/A	1
$(\rho_1, M = \pm 5)$	N/A	N/A	1	2
$(\rho_1, M = \pm 4)$	N/A	1	2	9
$(\rho_1, M = \pm 3)$	1	2	7	24
$(\rho_1, M = \pm 2)$	2	6	16	50
$(\rho_1, M = \pm 1)$	4	10	26	76
$(\rho_1, M = 0, \text{even}/Y^{\text{spin}})$	3	8	16	48
$(\rho_1, M = 0, \text{odd}/Y^{\text{spin}})$	3	5	16	42

modulus $S = n$ being maximal. Hence, $|\xi_{\boldsymbol{u}}\rangle$ is also an eigenstate of the Heisenberg Hamiltonian H_{H} [36, chapter 33], and its evolution under H_{H} leads to measurement probabilities that are all constant: $p_f^M = |\langle c_f^M|\psi(t)\rangle|^2 = \cos^{N+2M}(\theta/2)\sin^{N-2M}(\theta/2)$ for all states $|c_f^M\rangle$ in the basis $\mathcal{C}$ with total spin projection M.

The protocol $\mathcal{P}$ of section 2.2 yields time-dependent probabilities $p_f^M(t)$ for three possible combinations of initial states and Hamiltonians: (*i*) the initial state $|\psi_0\rangle = |\xi_{\boldsymbol{u}}\rangle$ evolving under the XXZ Hamiltonian with $J_z \neq J$; or the initial state $|\psi_0\rangle = |\chi_{\boldsymbol{u},\boldsymbol{v}}\rangle$ with $\boldsymbol{u} \neq \boldsymbol{v}$ evolving under (*ii*) the XXZ Hamiltonian or (*iii*) the Heisenberg Hamiltonian. These three cases are respectively considered in sections 5.1–5.3 below. Their discussion first requires the introduction of two observable consequences of the spatial and spin symmetries onto the time dependence of the measurement probabilities $p_f^M(t)$.

4. Observable consequences of symmetry on the time-dependent probabilities

From this point on, we choose the initial state used in the protocol ($\mathcal{P}$) of section 2.2 to be of the form of equation (3), i.e. $|\psi_0\rangle = |\chi_{\boldsymbol{u},\boldsymbol{v}}\rangle$. Under this assumption, we identify in sections 4.1 and 4.2 below two observable consequences of the spatial and spin symmetries onto the time dependence of the measurement probabilities $p_f^M(t) = |\langle c_f^M|\psi(t)\rangle|^2$, both of which may be verified on current experimental setups. (*A*) The first consequence concerns the qualitative behavior of the probabilities $p_f^M(t)$, which may be constant, oscillate sinusoidally, or undergo an aperiodic evolution. (*B*) The second consequence is that many probabilities $p_f^M(t)$ are equal at all times.

Both of these consequences follow from the fact that symmetries constrain the quantum evolution to occur within a subspace whose dimension is smaller than the number of possible measurement results. Indeed, owing to the conservations laws of section 3.2, the N-particle state $|\psi\rangle = \sum_{M=-n}^{n} |\psi^{\rho_1,M}\rangle$ is a sum of components $|\psi^{\rho_1,M}\rangle$. Each component evolves independently of the others, within the subspace (ρ_1, M) of Hilbert space comprised of all N-particle states which simultaneously (*i*) transform under the representation ρ_1 of D_{nh}, and (*ii*) are eigenstates of the operator S_z with the total spin projection M. Its dimension $\dim(\rho_1, M)$ is entirely determined by the symmetries of the Hamiltonian, independently of the values of the parameters J, J_z, and α entering equation (1). The component $|\psi^{\rho_1,M}(t)\rangle$ determines the probabilities $p_f^M(t) = |\langle c_f^M|\psi^{\rho_1,M}(t)\rangle|^2$ for all $\binom{N}{n+M}$ measurement results $|c_f^M\rangle$ in the basis $\mathcal{C}$ with total spin projection M.

We calculate the dimension $\dim(\rho_1, M)$ of each subspace (ρ_1, M) by constructing the projector onto it using well-established group-theoretical methods [27, § 94]. Our results for all four geometries of figure 1 and all allowed values of M are collected in table 1. They are noticeably smaller than $\binom{N}{n+M}$ (except if the total spin projection satisfies $|M| = n$).

We now derive the properties (*A*) and (*B*) announced at the beginning of the present section 4.

4.1. Qualitative behavior of the measurement probabilities

We first analyze the time dependence of the measurement probabilities $p_f^M(t) = |\langle c_f^M|\psi(t)\rangle|^2$. For that purpose, we introduce a basis $(|\Psi_\nu^{\rho,M}\rangle)$ of the Hilbert space $\mathcal{H}$, each of whose 2^N elements is an N-particle state which is an eigenstate of H with the energy $E_\nu^{\rho,M}$, an eigenstate of S_z with total spin projection M, and transforms according to the irreducible representation ρ of D_{nh}. All its components

$\langle c_f^M|\Psi_\nu^{\rho,M}\rangle$ may be chosen real (owing to the fact that all matrices U_ϕ of section 3.1 above and all characters of the irreducible representations of D_{nh} are real [27, § 94]). The probability amplitude $a_f^M(t) = \langle c_f^M|\psi(t)\rangle$ for the measurement at time t to yield the result $|c_f^M\rangle$, in the basis $\mathcal{C}$ with total spin projection M, reads:

$$a_f^M(t) = \sum_\nu a_{f,\nu}^M \exp\left(-\mathrm{i}\omega_\nu^M t\right) \ , \tag{4}$$

where the coefficient $a_{f,\nu}^M = \langle c_f^M|\Psi_\nu^{\rho_1,M}\rangle\langle\Psi_\nu^{\rho_1,M}|\psi_0\rangle$, the frequency $\omega_\nu^M = E_\nu^{\rho_1,M}/\hbar$, and the sum over ν includes all eigenstates $|\Psi_\nu^{\rho_1,M}\rangle$ of H in the subspace (ρ_1, M). For all cases considered in this article, the components $\langle c_f^M|\psi_0\rangle$ are all real, though this is not a requirement. Then, the coefficients $a_{f,\nu}^M$ are real, and the probability $p_f^M(t) = |a_f^M(t)|^2$ is given by:

$$p_f^M(t) = \sum_\nu \left(a_{f,\nu}^M\right)^2 + 2\sum_{\nu<\nu'} a_{f,\nu}^M a_{f,\nu'}^M \cos\left(\omega_{\nu,\nu'}^M t\right) \ , \tag{5}$$

where the transition frequency $\omega_{\nu,\nu'}^M = \omega_{\nu'}^M - \omega_\nu^M$. Equation (4) shows that, if the component $|\psi_0^M\rangle$ of the initial state with total spin projection M is non-zero, the time dependence of the probability amplitudes $\langle c_f^M|\psi(t)\rangle$ for all $\binom{N}{n+M}$ possible measurement results $|c_f^M\rangle$ with total spin projection M involve the same frequencies ω_ν^M, whose number is the dimension $d = \dim(\rho_1, M)$. Hence, the probabilities $p_f^M(t)$ of equation (5) all share the same qualitative behavior, piloted by d. If $d = 1$ (which holds for all geometries of figure 1 if $|M| = n$), the probabilities $p_f^M(t)$ for measurement results with total spin projection M are constant. If $d = 2$ (which holds for all geometries of figure 1 if $|M| = n-1$), the probabilities $p_f^M(t)$ all oscillate sinusoidally at the same frequency $\omega_{1,2}$. Finally, if $d \geqslant 3$, the probabilities $p_f^M(t)$ undergo an aperiodic evolution involving the same $d(d-1)/2$ frequencies $\omega_{\nu,\nu'}$, with $1 \leqslant \nu < \nu' \leqslant d$.

4.2. Equivalent and inequivalent measurement results

We now show that the spatial symmetries in D_{nh} cause many measurement probabilities $p_f^M(t)$ to be equal at all times. We consider two possible measurement results $|c_f^M\rangle$ and $|c_{f'}^M\rangle$ in the basis $\mathcal{C}$ with the same total spin projection M. We call them 'equivalent' if they correspond to each other through a spatial symmetry, i.e. $|c_{f'}^M\rangle = U_\phi|c_f^M\rangle$ for some ϕ in D_{nh}, the unitary operator U_ϕ being defined in section 3.1 above. The initial N-particle state $|\psi_0\rangle$ transforms under the unit representation ρ_1 of D_{nh}, hence, so does the state $|\psi(t)\rangle = \mathrm{e}^{-\mathrm{i}Ht/\hbar}|\psi_0\rangle$ just before the measurement. Therefore, the probability amplitude $\langle c_f^M|\psi(t)\rangle = \langle c_{f'}^M|U_\phi|\psi(t)\rangle = \langle c_{f'}^M|\psi(t)\rangle$. Thus, the probability amplitudes for equivalent measurement results are equal at all times, and, hence, so are the corresponding measurement probabilities, $p_f^M(t) = p_{f'}^M(t)$.

Measurement results which do not correspond through any symmetry operation are 'inequivalent'. For a given value of M, the number of different measurement probabilities $p_F^M(t)$ is equal to the number of inequivalent states $|c_F^M\rangle$ in the basis $\mathcal{C}$, labeled with a capital 'F'. We prove in appendix C, using a known result from group theory, that this number is equal to the dimension $\dim(\rho_1, M)$. This is the dimension of the subspace within which the component $|\psi^{\rho_1,M}(t)\rangle$ evolves. It is also equal to the number of frequencies entering equation (4) (see section 4.1 above). Hence, counting the number of different probabilities $p_F^M(t)$ gives direct access to this number of frequencies, without resorting to a Fourier transform.

For each of the different functions $p_F^M(t)$, the number N_F^M of equivalent measurement results $|c_f^M\rangle$ which share the same measurement probability $p_F^M(t)$ is also determined by the spatial symmetries. It is the number of distinct states $|c_f^M\rangle = U_\phi|c_F^M\rangle$, all in $\mathcal{C}$, obtained by acting on $|c_F^M\rangle$ using all spatial symmetry operators U_ϕ of section 3.1. The numbers N_F^M satisfy $\sum_{F=1}^{\dim(\rho_1,M)} N_F^M = \binom{N}{n+M}$.

5. Three cases within experimental reach

5.1. The state $|\xi_x\rangle$ evolving under H_{XXZ}

We first illustrate the results of section 4 above on the case of the initial state $|\psi_0\rangle = |\xi_{\boldsymbol{x}}\rangle = |\uparrow_1^x, \ldots, \uparrow_N^x\rangle$, which is the specific case of the states $|\xi_{\boldsymbol{u}}\rangle$, introduced in section 3.3, for the spherical coordinates $(\theta = \pi/2, \phi = 0)$. We let it evolve under the XXZ Hamiltonian (i.e. $J \neq J_z$ in equation (1)). The state $|\xi_{\boldsymbol{x}}\rangle$ is

not an eigenstate of H_{XXZ}, and the measurement probabilities $p_f^M(t)$ exhibit all three qualitative behaviors introduced in section 4.1 above, depending on the total projection M.

Constant probabilities for $M=\pm n$ — For any value of $N=2n$, the probabilities $p_f^{M=\pm n}=1/2^N$ for the two measurement results $|c_f^{M=\pm n}\rangle=|\uparrow_1^z,\ldots,\uparrow_1^z\rangle$ and $|\downarrow_1^z,\ldots,\downarrow_1^z\rangle$ are constant, owing to the subspaces $(\rho_1,M=\pm n)$ having dimension 1.

Sinusoidal oscillations for $M=\pm(n-1)$ — There are N possible measurement results in the basis $\mathcal{C}$ with total spin projection $M=n-1$. We label them $|c_f^{M=n-1}\rangle=|\uparrow_1^z\ldots\downarrow_f^z\ldots\uparrow_N^z\rangle$ with $1\leqslant f\leqslant N$, where the single $|\downarrow^z\rangle$ is located on site f: for $1\leqslant f\leqslant n$, it is on one of the sites of the outer ring, whereas for $n+1\leqslant f\leqslant N$, it is on the inner ring. The subspace $(\rho_1,M=n-1)$ has dimension 2, being spanned by the two states $|e_{\mathrm{outer}}^{M=n-1}\rangle=\sum_{f=1}^{n}|c_f^{M=n-1}\rangle/\sqrt{n}$ and $|e_{\mathrm{inner}}^{M=n-1}\rangle=\sum_{f=n+1}^{N}|c_f^{M=n-1}\rangle/\sqrt{n}$. The considerations of section 4 then yield the two following results. (*A*) The N measurement probabilities $p_f^{M=n-1}(t)=|\langle c_f^{M=n-1}|\psi(t)\rangle|^2$ all oscillate sinusoidally at the same frequency. (*B*) There are two inequivalent measurement results $|c_F^{M=n-1}\rangle$ with $F=1$ and 2, which may be chosen as, say, $|c_{f=1}^{M=n-1}\rangle$ and $|c_{f=n+1}^{M=n-1}\rangle$; all $(|c_f^{M=n-1}\rangle)_{1\leqslant f\leqslant n}$ share the same probability $p_1^{M=n-1}(t)$, whereas all $(|c_f^{M=n-1}\rangle)_{n+1\leqslant f\leqslant N}$ share the same probability $p_{n+1}^{M=n-1}(t)$. This behavior is a generalization of the Rabi oscillation [28, section IV.C.3] to the case of $N=2n$ spins. It affects the N measurement results with total spin projection $M=-(n-1)$ in the same way. It is a consequence of the double-ringed nature of the considered trapping geometries. It is not specific to the choice of the initial state, and we shall encounter it again in section 5.3 (see figure 6(a) below).

Aperiodic behavior for $1\leqslant|M|\leqslant n-2$ — We consider a value of the total spin projection M such that $1\leqslant|M|\leqslant n-2$. Then, for all considered geometries, $\dim(\rho_1,M)\geqslant 3$ (see table 1). Hence, the probabilities $p_f^M(t)=|\langle c_f^M|\psi(t)\rangle|^2$ exhibit an aperiodic dependence on t. The special case of $M=0$ requires further analysis and is presented in section 5.2 below.

Numerical results — Panels (a) and (b) of figure 3 respectively show the sinusoidal and aperiodic behaviors for the measurement probabilities $p_f^M(t)$ with $M=2$ and $M=1$, obtained numerically from the full $2^N\times 2^N$ Hamiltonian H_{XXZ} for $N=6$ particles, $J_z/J=-3$, and $\alpha=6$. Panels (d) and (e) confirm that, in both cases, the number of inequivalent measurement results $|c_F^M\rangle$ is equal to $\dim(\rho_1,M)$, and show the numbers N_F^M of states $|c_f^M\rangle$ equivalent to each of them. Our numerical results are in full agreement with our predictions of the previous paragraphs based on symmetry arguments alone.

Convention used for representing the probabilities — Panels (a)–(c) of figure 3 each focus on a given total spin projection M. We show a single curve per inequivalent measurement result $|c_F^M\rangle$, and represent the quantities $P_F^M(t)=p_F^M(t)\,N_F^M/\|\psi_0^M\|^2$, where $\|\psi_0^M\|^2=\langle\psi_0^M|\psi_0^M\rangle$, and $|\psi_0^M\rangle$ is the component of $|\psi_0\rangle$ with total spin projection M. These are the total probabilities for each set of equivalent measurement results, rescaled such that $\sum_F P_F^M(t)=1$. The same convention is used for figures 4 and 6 discussed below.

5.2. XXZ Hamiltonian: two-fold rotation of the N spins

The conservation laws stated in section 3.2 account for all spatial symmetries in D_{nh} and spin rotations about the axis $\boldsymbol{z}$ through arbitrary angles. However, for some choices of the Hamiltonian and initial state, additional spin symmetries come into play. Then, the numbers of frequencies and inequivalent measurement results obtained in section 4 are overestimates, which may be refined. The case of the initial state $|\xi_{\boldsymbol{u}}\rangle$ evolving under the Heisenberg Hamiltonian, discussed in section 3.3 above, is a simple example. In this case, the conservation of $\boldsymbol{S}^2$ entails that the component $|\psi^{\rho_1,M}(t)\rangle$ of the N-particle state $|\psi(t)\rangle$ with total spin projection M is proportional to the single eigenstate of H_H in the subspace (ρ_1,M) with maximal total spin modulus $S=n$: thus, for a given M, all probabilities $p_f^M=|\langle c_f^M|\psi(t)\rangle|^2$ are constant and equal.

We now consider the spin rotation $g=C_\theta^{\boldsymbol{e}}$ through the angle θ about an arbitrary axis $\boldsymbol{e}$ in the horizontal plane (xy). For the Heisenberg Hamiltonian, $C_\theta^{\boldsymbol{e}}$ is an element of the spin symmetry group G^{spin} of section 3.1 above for any angle θ, leading to the conservation of the operator $\boldsymbol{e}\cdot\boldsymbol{S}$. By contrast, for the XXZ Hamiltonian, $C_\theta^{\boldsymbol{e}}$ is in G^{spin} only for $\theta=0$ or π. In the remainder of the present section 5.2, we focus on the XXZ case and identify the parity conservation law corresponding to these spin rotations. We demonstrate its role by comparing the measurement probabilities obtained from three different initial states, discussing both their time dependence and their Fourier transform.

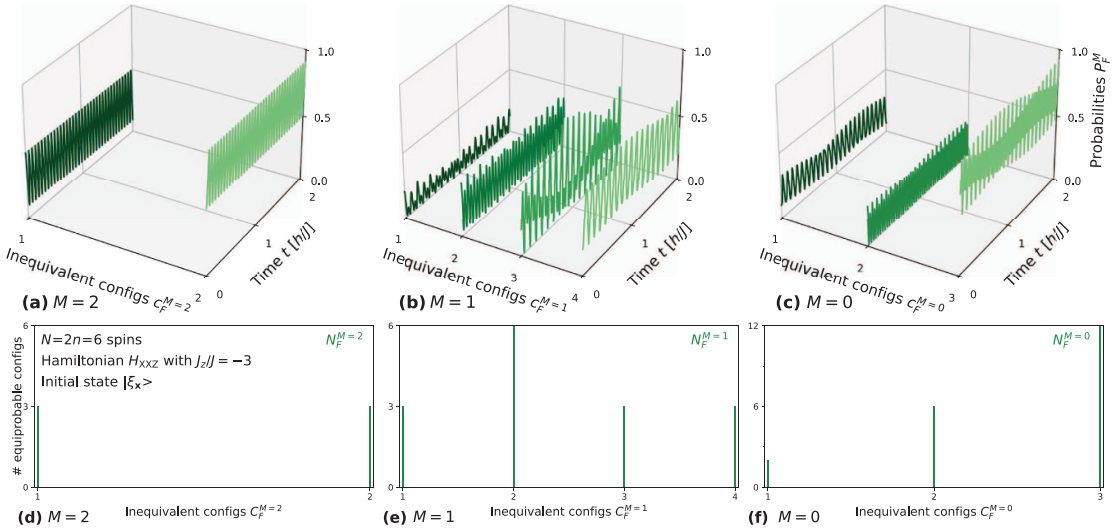


Figure 3. Panels (a)–(c): Time-dependent probabilities for the inequivalent measurement results $|c_F^M\rangle$ with total spin projection M, for the initial state $|\psi_0\rangle = |\xi_x\rangle$ involving $N = 6$ particles, evolving under the Hamiltonian H_{XXZ} with $J_z/J = -3$ and $\alpha = 6$, for $M = 2$ (a), 1 (b), and 0 (c). For each value of M, we represent the quantities $P_F^M(t) = p_F^M(t)\, N_F^M/\|\psi_0^M\|^2$, as defined in section 5.1. Panels (d)–(f) show the numbers N_F^M of equivalent measurement results having probability $p_F^M(t)$.

5.2.1. Parity under Y_{spin} for quantum states with $M = 0$

We consider the spin rotation $g = C_\pi^y$ through angle π about the axis $\boldsymbol{y}$. The operator Y_{spin}, which acts on the Hilbert space $\mathcal{H}$ and represents g, reads (see section 3.1 above):

$$Y_{\text{spin}} = U_g = (-\mathrm{i}\sigma_1^y)\ldots(-\mathrm{i}\sigma_N^y)\ . \tag{6}$$

The operator $Y_{\text{spin}}^2 = 1$, because the system is comprised of an even number $N = 2n$ of spins–1/2 [27, § 99]. Thus, Y_{spin} represents a two-fold rotation of the N spins.

We focus on the subspace $(\rho_1, M = 0)$ defined in section 4, which is invariant under Y_{spin}. It is the direct sum of two subspaces, $(\rho_1, M = 0) = (\rho_1, M = 0, \text{even}/Y_{\text{spin}}) \oplus (\rho_1, M = 0, \text{odd}/Y_{\text{spin}})$, respectively comprised of the eigenstates of Y_{spin} with eigenvalue $+1$ (states which are even under Y_{spin}, denoted even$/Y_{\text{spin}}$) and -1 (states which are odd under Y_{spin}, denoted odd$/Y_{\text{spin}}$). The dimensions of these two subspaces are given in table 1 for all four geometries of figure 1. We prove in appendix C.2 that all spin rotations $C_\pi^{\boldsymbol{e}}$ through angle π about an arbitrary axis $\boldsymbol{e}$ in the (xy) plane act on states with total spin projection $M = 0$ as the operator Y_{spin} of equation (6) and, hence, lead to the same definition of parity.

The parity with respect to Y_{spin} is conserved during the evolution described by the Schrödinger equation. However, the possible measurement results $|c_f^{M=0}\rangle$ in the basis $\mathcal{C}$ each have both even and odd components under Y_{spin}, respectively given by $(1 \pm Y_{\text{spin}})\,|c_f^{M=0}\rangle/\sqrt{2}$. Thus, in general, the probability amplitudes $\langle c_f^{M=0}|\psi(t)\rangle$ result from the interference between the components of $|\psi(t)\rangle$ along the even and odd subspaces. Extending the idea introduced in section 3.3 above, we avoid this interference by choosing initial states $|\psi_0\rangle$ whose components $|\psi_0^{M=0}\rangle$ with total spin projection $M = 0$ are eigenstates of Y_{spin}. We show in appendix B that, among the states $|\chi_{\boldsymbol{u},\boldsymbol{v}}\rangle$ of the form of equation (3), only two families of states satisfy this property. Both families are defined in terms of one arbitrary unit vector $\boldsymbol{u}$ representing a direction on the Bloch sphere: (*i*) the states $|\xi_{\boldsymbol{u}}\rangle = |\chi_{\boldsymbol{u},\boldsymbol{u}}\rangle$ introduced in section 3.3, and (*ii*) the states $|\eta_{\boldsymbol{u}}\rangle = |\chi_{\boldsymbol{u},\boldsymbol{u}'}\rangle$, where the unit vector $\boldsymbol{u}'$ is the image of $\boldsymbol{u}$ under the rotation through angle π about the axis $\boldsymbol{z}$. The components $|\xi_{\boldsymbol{u}}^{M=0}\rangle$ and $|\eta_{\boldsymbol{u}}^{M=0}\rangle$ are eigenstates of Y_{spin} corresponding to the eigenvalues $(-1)^n$ and $+1$, respectively.

If the initial states $|\psi_0\rangle = |\xi_{\boldsymbol{u}}\rangle$ or $|\eta_{\boldsymbol{u}}\rangle$ are chosen in the protocol $(\mathcal{P})$, the consequences (A) and (B) of symmetry described in section 4 are strengthened as follows. (A) The number of different frequencies entering the probability amplitudes $\langle c_f^{M=0}|\psi(t)\rangle$ with total spin projection $M = 0$, given by equation (4), and (B) the number of inequivalent measurement results $|c_f^{M=0}\rangle$, are both equal to the dimension $d = \dim(\rho_1, M = 0, \text{even}/Y_{\text{spin}})$. For odd values of n, this dimension is also equal to $\dim(\rho_1, M = 0, \text{odd}/Y_{\text{spin}})$ (see table 1). We prove these properties in appendix C. We have checked them numerically in all four geometries of figure 1. In particular, our numerical results for the initial state $|\xi_{\boldsymbol{x}}\rangle$ in the geometry with $N = 2n = 6$, and with the same parameters as in section 5.1, are shown on

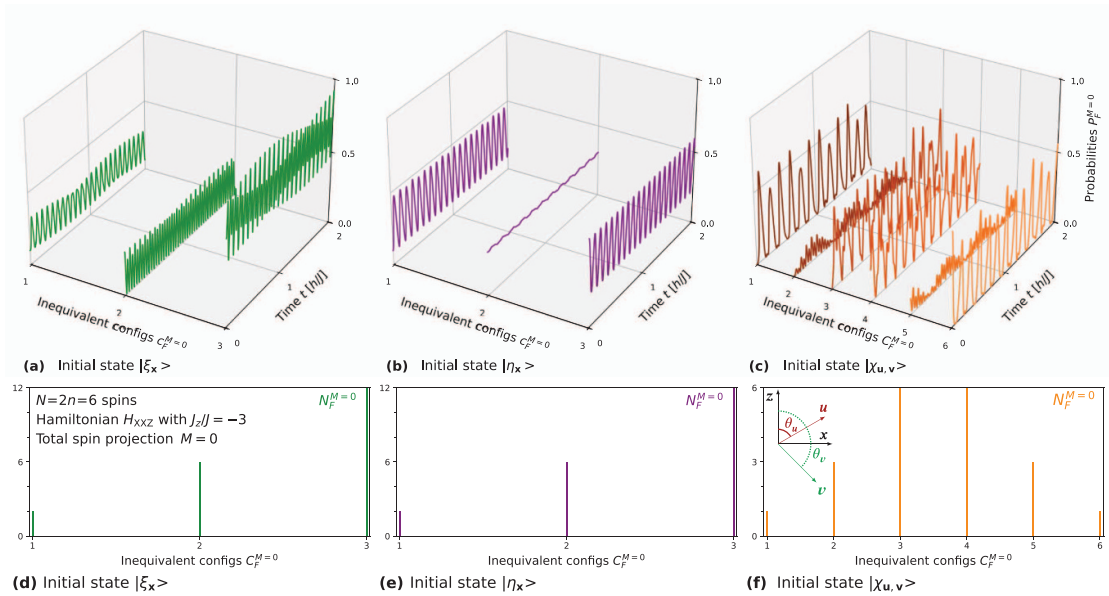


Figure 4. Panels (a)–(c): Time-dependent probabilities for the inequivalent measurement results $|c_F^{M=0}\rangle$ with total spin projection $M=0$, for the initial states $|\psi_0\rangle = |\xi_{\boldsymbol{x}}\rangle$ (a), $|\eta_{\boldsymbol{x}}\rangle$ (b), and $|\chi_{\boldsymbol{u},\boldsymbol{v}}\rangle$ (c). The unit vectors $\boldsymbol{u}$ and $\boldsymbol{v}$ on the Bloch sphere are chosen in the $(\boldsymbol{x},\boldsymbol{z})$ plane with angles $\theta_{\boldsymbol{u}} = \pi/3$ and $\theta_{\boldsymbol{v}} = 3\pi/4$ [see inset to panel (f)]. All states involve $N=6$ particles, and evolve under the Hamiltonian H_{XXZ} with $J_z/J=-3$ and $\alpha=6$. In each case, we represent the quantities $P_F^{M=0}(t) = p_F^{M=0}(t)\, N_F^{M=0}/\|\psi_0^{M=0}\|^2$ (see section 5.1). Panels (d)–(f) show the numbers $N_F^{M=0}$ of equivalent measurement results having probability $p_F^{M=0}(t)$. [Panels (a), (d) of this figure coincide with panels (c), (f) of figure 3.].

panels (c) and (f) of figure 3: they confirm the presence of $\dim(\rho_1, M=0, \mathrm{even}/Y_{\mathrm{spin}}) = 3$ [rather than $\dim(\rho_1, M=0) = 6$] inequivalent measurement results.

To summarize, three different cases are accessible using initial states $|\psi_0\rangle = |\chi_{\boldsymbol{u},\boldsymbol{v}}\rangle$ of the form of equation (3): (*i*) n even, $|\psi_0^{M=0}\rangle$ even under Y_{spin}; (*ii*) n odd, $|\psi_0^{M=0}\rangle$ even under Y_{spin}; (*iii*) n odd, $|\psi_0^{M=0}\rangle$ odd under Y_{spin}. In all cases, (A) the number of frequencies entering the probability amplitudes $\langle c_f^{M=0}|\psi(t)\rangle$ and (B) the number of inequivalent measurement results are both equal to the dimension of the subspace within which the component $|\psi^{M=0}(t)\rangle$ evolves, as in section 4.2. The additional conservation law of parity under Y_{spin} further constrains the dimension of this subspace, which is now $(\rho_1, M=0, \mathrm{even}/Y_{\mathrm{spin}})$ or $(\rho_1, M=0, \mathrm{odd}/Y_{\mathrm{spin}})$.

5.2.2. Case of odd n: three different initial states evolving under H_{XXZ}

In this section, we identify observable consequences of the conservation of parity under Y_{spin}. In particular, we show how to demonstrate the fact that initial states with total spin projection $M=0$ which are even or odd under Y_{spin} give rise to quantum dynamics occurring within the different subspaces $(\rho_1, M=0, \mathrm{even}/Y_{\mathrm{spin}})$ or $(\rho_1, M=0, \mathrm{odd}/Y_{\mathrm{spin}})$, respectively. We consider the initial states $|\xi_{\boldsymbol{u}}\rangle$ and $|\eta_{\boldsymbol{u}}\rangle$, which are the only N-particle states of the form of equation (3) whose $M=0$ component is an eigenstate of Y_{spin} (see section 5.2.1 above). The direction $\boldsymbol{u}$ may be chosen arbitrarily on the Bloch sphere. For even values of n, the components $|\xi_{\boldsymbol{u}}^{M=0}\rangle$ and $|\eta_{\boldsymbol{u}}^{M=0}\rangle$ are both even under Y_{spin}, so that odd states are inaccessible with the considered initial states, and the dynamics of even and odd states may not be compared. By contrast, for odd values of n, $|\xi_{\boldsymbol{u}}^{M=0}\rangle$ and $|\eta_{\boldsymbol{u}}^{M=0}\rangle$ are respectively odd and even under Y_{spin}. Therefore, we focus on the case of odd n and compare the measurement probabilities obtained from these two states.

Time dependence — In figure 4, we compare the probabilities $p_f^{M=0}(t)$ for the measurement results with total spin projection $M=0$, for the geometry involving $N=2n=6$ spins, and for three different initial states $|\psi_0\rangle = |\xi_{\boldsymbol{x}}\rangle$, $|\eta_{\boldsymbol{x}}\rangle$, and $|\chi_{\boldsymbol{u},\boldsymbol{v}}\rangle$. For the state $|\chi_{\boldsymbol{u},\boldsymbol{v}}\rangle$, the directions $\boldsymbol{u}$ and $\boldsymbol{v}$ on the Bloch sphere are chosen in the (x,z) plane, the angles $\theta_{\boldsymbol{u}} = \pi/3$ and $\theta_{\boldsymbol{v}} = 3\pi/4$ being defined in the inset to figure 4(f). These three initial states evolve under the same Hamiltonian H_{XXZ}. The parameters J, J_z and α entering equation (1) are the same as in figure 3, so that panels (a,d) of figure 4 coincide with panels (c),(f) of figure 3. The components $|\xi_{\boldsymbol{x}}^{M=0}\rangle$ and $|\eta_{\boldsymbol{x}}^{M=0}\rangle$ each give rise to 3 inequivalent measurement results $|c_F^{M=0}\rangle$ (see panels d, e of figure 4), in agreement with our prediction of section 5.2.1. By contrast, the component $|\chi_{\boldsymbol{u},\boldsymbol{v}}^{M=0}\rangle$, which is not an eigenstate of Y_{spin}, yields six inequivalent measurement results (panels c and f), in accordance with the result of section 4.2.

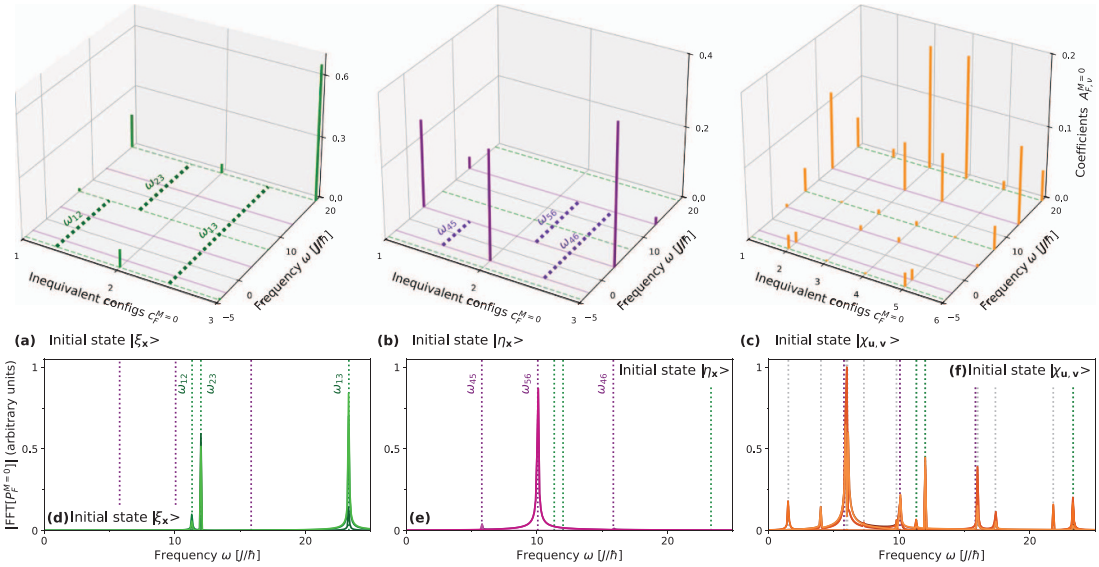


Figure 5. Panels (a)–(c): Fourier transforms of the probability amplitudes $\langle c_F^{M=0}|\psi(t)\rangle$ obtained for the initial states and Hamiltonians of figure 4. We represent the quantities $A_{F,\nu}^{M=0} = N_F^{M=0}\,(a_{F,\nu}^{M=0}/\|\psi_0^{M=0}\|)^2$, introduced in section 5.2.2, as a function of the frequencies $\omega_\nu^{M=0}$. The energies $\hbar\omega_\nu^{M=0}$ of the eigenstates of $H_{\rm XXZ}$ which are odd and even under the operator $Y_{\rm spin}$ are respectively shown as thin green and purple horizontal lines on the bases of the three plots. The thick dashed lines on the bases of (a) and (b) show the transition frequencies $\omega_{\nu,\nu'}$ respectively allowed for $|\xi_{\boldsymbol{x}}\rangle$ and $|\eta_{\boldsymbol{x}}\rangle$. [The scales along the vertical axes of the three panels (a)–(c) are different.] Panels (d)–(f): absolute values of the fast Fourier transforms (FFT) of the corresponding probabilities $P_F^{M=0}(t)$ for $0\leqslant t\leqslant t_{\rm max} = 10\,h/J$, all superimposed (only the positive frequencies are represented). The transition frequencies $\omega_{\nu,\nu'}$ allowed for $|\xi_{\boldsymbol{x}}\rangle$ and $|\eta_{\boldsymbol{x}}\rangle$ are shown as the vertical green and purple lines. All other transition frequencies are shown in gray on panel (f).

Fourier transform — We now identify an observable signature of the fact that initial states whose $M=0$ components, $|\psi_0^{M=0}\rangle$, are even or odd under $Y_{\rm spin}$, yield quantum evolutions for $|\psi^{M=0}(t)\rangle$ occurring within different subspaces. We introduce the Fourier transform $\widetilde{f}(\omega) = \int_{-\infty}^{\infty} {\rm d}t\, {\rm e}^{{\rm i}\omega t} f(t)/(2\pi)$ of any function of time $f(t)$. The Fourier transform $\widetilde{a}_f^M(\omega)$ of the probability amplitude $a_f^M(t)$ of equation (4) reads, for $M=0$,

$$\widetilde{a}_f^{M=0}(\omega) = \sum_\nu a_{f,\nu}^{M=0}\,\delta(\omega-\omega_\nu^{M=0})\ . \tag{7}$$

The frequencies $\omega_\nu^{M=0} = E_\nu^{\rho_1,M=0}/\hbar$ entering equation (7) are determined by the eigenvalues of $H_{\rm XXZ}$ for the eigenstates in the subspace $(\rho_1, M=0)$, which do not depend on the initial state $|\psi_0\rangle$. By contrast, the coefficients $a_{f,\nu}^{M=0}$ are proportional to $\langle\Psi_\nu^{\rho_1,M=0}|\psi_0\rangle$ (see section 4.1) and, hence, do depend on $|\psi_0\rangle$. The eigenstates $|\Psi_\nu^{\rho_1,M=0}\rangle$ may each be chosen to be either even or odd under $Y_{\rm spin}$. Thus, if $|\psi_0^{M=0}\rangle$ is even (resp. odd) under $Y_{\rm spin}$, only even (resp. odd) eigenstates take part in equation (7), and $\widetilde{a}_f^{M=0}(\omega)$ is non-zero only for the corresponding subset of frequencies $\omega_\nu^{M=0}$. By contrast, if $|\psi_0^{M=0}\rangle$ is not an eigenstate of $Y_{\rm spin}$, all frequencies $\omega_\nu^{M=0}$ take part in the sum.

The Fourier transform $\widetilde{p}_f^{M=0}(\omega)$ of the probability $p_f^{M=0}(t)$ given by equation (5), reflects the parity of $|\psi_0^{M=0}\rangle$ under $Y_{\rm spin}$ similarly. If $|\psi_0^{M=0}\rangle$ is even (resp. odd), the Fourier transform $\widetilde{p}_f^{M=0}(\omega)$ only involves transition frequencies $\omega_{\nu,\nu'}$ corresponding to pairs of eigenstates $|\Psi_\nu^{\rho_1,M=0}\rangle$ and $|\Psi_{\nu'}^{\rho_1,M=0}\rangle$ which are both even (resp. odd) under $Y_{\rm spin}$. By contrast, if $|\psi_0^{M=0}\rangle$ is not an eigenstate of $Y_{\rm spin}$, the transition frequencies corresponding to all pairs of eigenstates in the $(\rho_1, M=0)$ subspace, regardless of their parity, may enter $\widetilde{p}_f^{M=0}(\omega)$.

These predictions are fully confirmed by our numerical results illustrated in figure 5. Its panels (a)–(c) show the coefficients $a_{f,\nu}^{M=0}$ entering equation (7) above as a function of the frequencies $\omega_\nu^{M=0}$, for the three initial states of figure 4, all evolving under the Hamiltonian $H_{\rm XXZ}$ with the same parameters. In each case, we show a single set of coefficients per inequivalent result $|c_F^{M=0}\rangle$, and represent the quantities $A_{F,\nu}^{M=0} = N_F^{M=0}\,(a_{F,\nu}^{M=0})^2/\|\psi_0^{M=0}\|^2$, whose sum over F and ν is 1. The state $|\xi_{\boldsymbol{x}}\rangle$, whose $M=0$ component is odd under $Y_{\rm spin}$, has non-zero coefficients $a_{F,\nu}^{M=0}$ only for the three frequencies $\omega_\nu^{M=0} = E_\nu^{\rho_1,M=0}/\hbar$ corresponding to eigenstates of $H_{\rm XXZ}$ which are odd under $Y_{\rm spin}$, shown as the thin dashed green lines on the base of each plot. The state $|\eta_{\boldsymbol{x}}\rangle$, whose $M=0$ component is even under $Y_{\rm spin}$, has non-zero coefficients $a_{F,\nu}^{M=0}$ only for the three frequencies $\omega_\nu^{M=0}$ corresponding to even eigenstates, shown as the

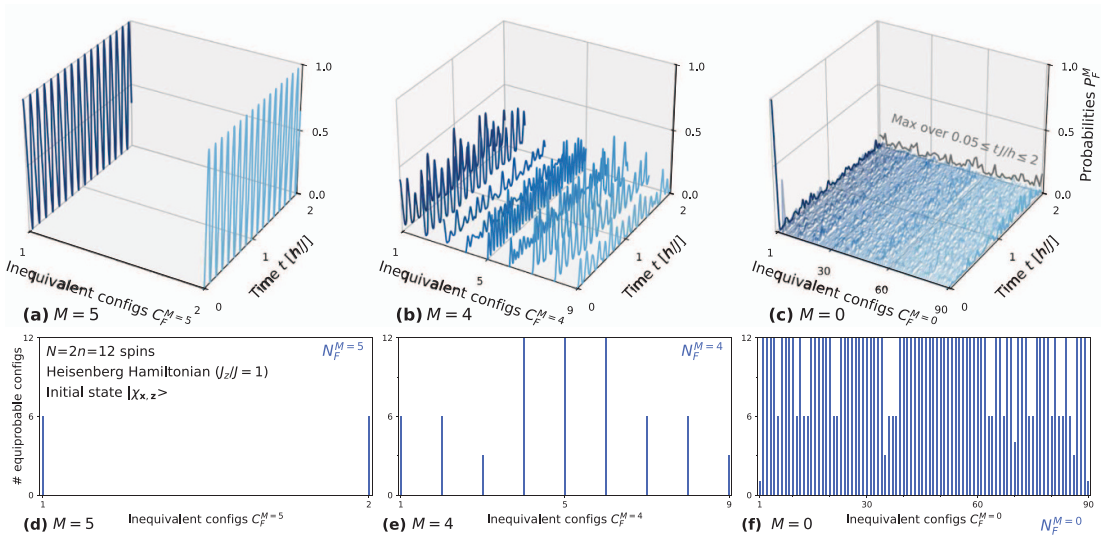


Figure 6. Time-dependent probabilities for the inequivalent measurement results $|c_F^M\rangle$ with total spin projection M, for the initial state $|\psi_0\rangle = |\chi_{\boldsymbol{x},\boldsymbol{z}}\rangle$ involving $N = 12$ particles, evolving under the Heisenberg Hamiltonian with $\alpha = 6$, for $M = 5$ (a), 4 (b), and 0 (c). For each M, we represent the ratios $P_F^M(t) = p_F^M(t)\, N_F^M/\|\psi_0^M\|^2$. The gray curve on the back face of panel (c) shows the maximum value of each $P_F^{M=0}(t)$ over the time interval $0.05 \leqslant tJ/h \leqslant 2$. Panels (d)–(f) show the numbers N_F^M of equivalent measurement results having probability $p_F^M(t)$.

thin solid purple lines. By contrast, the state $|\chi_{\boldsymbol{u},\boldsymbol{v}}\rangle$ has non-zero coefficients $a_{F,\nu}^{M=0}$ for all six eigenstates. Panels (d)–(f) represent the fast Fourier transform (FFT)[2] of the probabilities $P_F^{M=0}(t)$ over the time interval $0 \leqslant t \leqslant t_{\max}$ with $t_{\max} = 10h/J$, for the inequivalent results $|c_F^{M=0}\rangle$, all superimposed. Panel (d) exhibits three peaks, corresponding to the three transition frequencies ω_{12}, ω_{23}, ω_{31} between odd states, shown by the vertical dashed green lines and identified on the base of panel (a). Panel (e) shows one dominant peak for ω_{56} and two smaller ones for ω_{45} and ω_{46}, corresponding to the three transition frequencies between even states, shown by the vertical dashed purple lines and identified on the base of panel (b). Finally, panel (f) shows numerous peaks, some occurring for transition frequencies involving even or odd states, and others for transition frequencies involving an even state and an odd one, shown by the vertical dashed gray lines.

The peaks of panels (d) occur for frequencies $(\omega_{12}, \omega_{23}, \omega_{31})$ which are all different from those of panel (e), namely, $(\omega_{45}, \omega_{56}, \omega_{64})$. This provides the sought signature of the quantum evolution within different subspaces for initial states whose component $|\psi_0^{M=0}\rangle$ is odd or even under Y_{spin}. Panel (f) further illustrates that, if $|\psi_0^{M=0}\rangle$ is not an eigenstate of Y_{spin}, the measurement performed at time t causes interference between the even and odd components of $|\psi^{M=0}(t)\rangle$. All these predictions may readily be tested in experiments by taking the FFT of the time-dependent measurement probabilities $p_F^{M=0}(t)$.

Fourier analysis and finite observation time — The positive-frequency components of the Fourier transform of equation (5) are Dirac peaks at the frequencies $\omega_{\nu,\nu'}^{M=0}$, shown as the vertical dashed lines in panels (d)–(f) of figure 5. In the FFT results (solid curves), owing to the finite duration $t_{\max}$ of the time interval which is accounted for, the peaks acquire a non-zero width $\Delta\omega \approx 4\pi/t_{\max}$ [39, figure 6.2(d)], so that $\hbar\Delta\omega/J \approx 0.2$ in figures 5(d)–(f). This width is sufficiently small for all 3 transition frequencies between odd states [panel (d)] and all 3 transition frequencies between even states [panel (e)] to be clearly resolved. On panel (f) (expected number of transition frequencies: $6 \times 5/2 = 15$, see table 1), a few nearby frequencies remain unresolved, but the FFT signals still exhibit 10 peaks, confirming that transitions do occur between even and odd states. The time $t_{\max} = 10h/J$, also used in figures 7(b) and (d) below, is within reach for the experimental proposal of [21, section II and App. A].

5.3. For larger spin numbers N: collapse of the initial state

5.3.1 Evolution under the Heisenberg Hamiltonian

In this section, we choose the N-particle initial state $|\psi_0\rangle = |\chi_{\boldsymbol{x},\boldsymbol{z}}\rangle$, given by equation (3) with $\boldsymbol{u} = \boldsymbol{x}$ and $\boldsymbol{v} = \boldsymbol{z}$, and let the system evolve under the Heisenberg Hamiltonian.

[2] All numerical calculations presented in this article have been performed using the Python libraries NumPy [37] and SciPy [38]. In particular, the FFT spectra of figures 5(d)–(f) have been obtained using the function `rfft` in SciPy.

For total spin projections $M > 0$, the resulting measurement probabilities $p_F^M(t)$ behave in a very similar way as those obtained from the initial state $|\xi_{\boldsymbol{x}}\rangle$ evolving under the XXZ Hamiltonian (see section 5.1 above). Specifically, the single probability with maximal $M = n$ is constant; the N probabilities with $M = n-1$, among which two are inequivalent, oscillate sinusoidally; the probabilities $p_F^M(t)$ with $1 \leqslant M \leqslant n-2$ undergo an aperiodic evolution. These predictions are confirmed by our numerical results for $N = 12$ spins, illustrated in figure 6 for $N = 2n = 12$ spins. Its panels (a) and (b) show the sinusoidal and aperiodic behaviors expected for $M = 5$ and 4, respectively, and the corresponding panels (d) and (e) show the numbers of equivalent measurement results N_F^M. They are directly comparable to panels (a),(b) and (d),(e) of figure 3 above.

Despite the choice of the Hamiltonian H_{H}, these results exhibit no straightforward signature of the conservation of the total spin modulus S. This is because the component $|\chi_{\boldsymbol{x},\boldsymbol{z}}^M\rangle$ of the initial state with total spin projection M is not an eigenstate of the squared total spin operator $\boldsymbol{S}^2$ (except for $|M| = n$). In particular, the sinusoidal regime of $M = n-1$ involves two eigenstates of H_{H} with $S = n$ and $S = n-1$, respectively. These states are not coupled during the evolution described by the Schrödinger equation. However, the measurement at time t causes them to interfere, because the configurations $|c_f^{M=n-1}\rangle$ have non-zero components with both $S = n$ and $S = n-1$.

5.3.2. Collapse of the $M = 0$ component of the initial state

We retain the initial state $|\chi_{\boldsymbol{x},\boldsymbol{z}}\rangle$ evolving under the Heisenberg Hamiltonian, and turn to the probabilities $p_F^{M=0}(t)$ for the measurement results $|c_F^{M=0}\rangle$ with total spin projection $M = 0$. They exhibit a specific qualitative behavior, dictated by the two following properties. Firstly, the component $|\chi_{\boldsymbol{x},\boldsymbol{z}}^{M=0}\rangle$ of the initial state reads:

$$|\chi_{\boldsymbol{x},\boldsymbol{z}}^{M=0}\rangle = \frac{1}{2^{n/2}}\,|{\downarrow_1^z},\ldots{\downarrow_n^z};{\uparrow_{n+1}^z},\ldots,{\uparrow_N^z}\rangle = \frac{1}{2^{n/2}}\,|c_1^{M=0}\rangle\ , \tag{8}$$

the configurations $|c_F^M\rangle$ being numbered as in appendix A. Equation (8) shows that $|\chi_{\boldsymbol{x},\boldsymbol{z}}^{M=0}\rangle$ is proportional to the single configuration $|c_1^{M=0}\rangle$. Secondly, for larger values of N, the dimension $\dim(\rho_1, M=0)$ increases. For example, this dimension is $48+42 = 90$ for $N = 12$ (see table 1).

The combination of these two properties yields the collapse of the initial component $|\chi_{\boldsymbol{x},\boldsymbol{z}}^{M=0}\rangle$, illustrated in figure 6(c) for $N = 2n = 12$. We now discuss this specific case. Initially, the only configuration $|c_F^{M=0}\rangle$ with non-zero probability is $|c_1^{M=0}\rangle$. Thus, the quantity $P_1^{M=0}(t)$, introduced in section 5.1 and represented in figure 6(c), satisfies $P_1^{M=0}(0) = 1$, and all other $P_F^{M=0}(0) = 0$. The value of $P_1^{M=0}(t)$ strongly decreases over a very short time t, and after a transient regime whose duration is of the order of $0.05h/J$, the quantities $P_F^{M=0}(t)$ for all inequivalent measurement results $|c_F^{M=0}\rangle$ remain < 0.15 for all times up to $t_{\max} = 2h/J$, as shown by the gray curve on the back face of figure 6. The quantities $P_F^{M=0}(t)$ corresponding to different numbers of equivalent probabilities $N_F^{M=0}$ (shown in figure 6(f) have comparable magnitudes. In particular, nine quantities $P_F^{M=0}(t)$ exceed 0.1 at least once over the time interval $0.05h/J < t < 2h/J$, with $N_F^{M=0}$ equal to 1, 6, or 12.

Our numerical results show no revival of the initial state for longer durations up to $t_{\max} = 10h/J$.

5.3.3. Comparison of various system sizes and Hamiltonians

Finally, starting from the same initial state $|\chi_{\boldsymbol{x},\boldsymbol{z}}\rangle$ as in section 5.3.2 above, we seek to optimize the observation of the collapse by varying the number of spins $N = 2n$ or the ratio J_z/J entering the Hamiltonian of equation (1). We characterize the quality of the collapse by the maximum $Q = \max[P_F^{M=0}(t)]$, taken over all inequivalent measurement results $|c_F^{M=0}\rangle$ with total spin projection $M = 0$, and all times t such that $0.05\,h/J \leqslant t \leqslant t_{\max}$, where $t_{\max} = 2\,h/J$ or $10\,h/J$. Lower values of Q signal a higher quality for the collapse.

Our results are summarized in figure 7. We first assume that the system evolves under the Heisenberg Hamiltonian. In this case, panels (a,b) show that increasing N leads to lower values of Q, in accordance with the fact that $\dim(\rho_1, M=0)$ increases with N (see table 1). Hence, the collapse will be investigated more efficiently with larger systems. Next, we consider the geometry of figure 1(d) involving $N = 12$ spins. Panel (c) indicates that, for the shorter duration $t_{\max} = 2\,h/J$, the lowest value of Q is achieved using the Heisenberg Hamiltonian. However, for the longer duration $t_{\max} = 10\,h/J$, panel (d) reveals that the Heisenberg Hamiltonian is no longer optimal, and suggests turning to the more general XXZ Hamiltonian with smaller values of the ratio J_z/J.

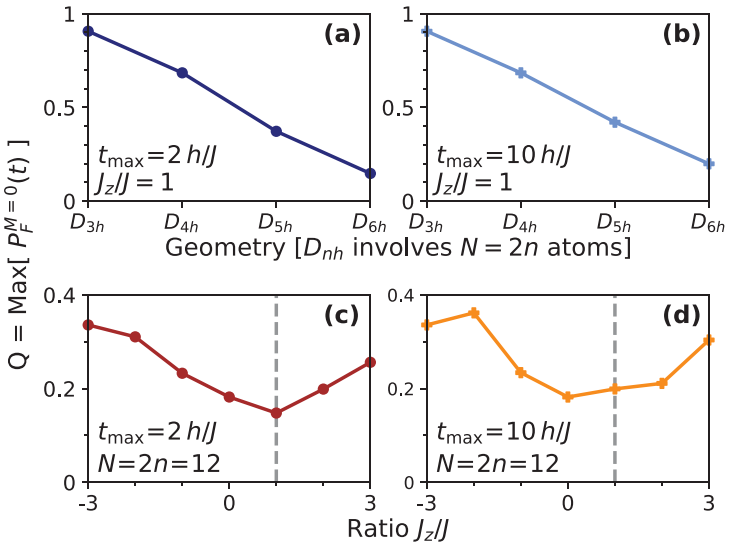


Figure 7. Collapse of the component of the initial state $|\psi_0\rangle = |\chi_{x,z}\rangle$ with total spin projection $M=0$. On each panel, we represent the maximum Q of the quantities $P_F^{M=0}(t) = p_F^{M=0}(t)\, N_F^{M=0}/\|\psi_0^{M=0}\|^2$ over all inequivalent measurement results with $M=0$ and times t such that $0.05\,h/J \leqslant t \leqslant t_{max}$. On panels (a), (b), we compare the four systems of figure 1 evolving under the Heisenberg Hamiltonian ($J_z/J=1$). On panels (c), (d), we consider the system comprised of $N=2n=12$ spins, and vary the ratio J_z/J from -3 to 3 (the dashed gray line shows the Heisenberg value $J_z/J=1$). The maximum time $t_{max}=2\,h/J$ for panels (a), (c) and $10\,h/J$ for panels (b), (d).

6. Conclusion

We have theoretically analyzed the time dependence of the measurement probabilities obtained on an XXZ quantum simulator comprised of up to $N=2n=12$ interacting particles trapped in a planar geometry with high spatial symmetry, namely, point group symmetry D_{nh}. We consider experimentally accessible initial states which are invariant under all spatial symmetries, i.e. which transform under the unit representation ρ_1 of the spatial symmetry group. Then, the quantum evolution of the component of the N-particle wavefunction with total spin projection M takes place within the subspace (ρ_1, M) of section 4. In the case of section 5.2, where the parity under Y_{spin} plays a role, the relevant subspaces are $(\rho_1, M=0, \text{even}/Y_{spin})$ and $(\rho_1, M=0, \text{odd}/Y_{spin})$. The dimensions of these subspaces, collected in table 1, determine the qualitative behavior of the time dependence of the measurement probabilities, and are equal to the number of inequivalent measurement results. These dimensions, calculated using group-theoretical methods, are characteristic of the spin-point symmetry group of the Hamiltonian: our protocol may be understood as a way of determining them experimentally.

The protocol we have put forward is within experimental reach, e.g. with trapped Rydberg atoms or polar molecules, owing to recent advances in trapping techniques [11], in the quantum simulation of spin Hamiltonians [20, 22] and in the implementation of projective quantum measurements [23]. Our protocol involves initial states that are easy to prepare, and relies on the measurement scheme whose experimental implementation is the most straightforward, namely, the simultaneous measurement of the z-component of all N effective spins.

We have highlighted two predictions. Firstly, the XXZ Hamiltonian is invariant under a twofold rotation of the N spins about an axis in the horizontal plane. This yields a conservation law which may be probed efficiently in smaller systems involving e.g. $N=6$ spins (see section 5.2). The second highlighted prediction concerns larger systems (e.g. $N=12$ spins, see section 5.3). There, four different qualitative behaviors may be observed for the time dependence of the measurement probabilities: these may be constant, or oscillate sinusoidally, or undergo an aperiodic evolution, or exhibit the collapse of the component of the initial state with total spin projection $M=0$. These four behaviors are observed on the same system, prepared in the same initial state, using the same values for the parameters J and J_z entering the Hamiltonian of equation (1). Each realization of the protocol will explore a subspace with given spin projection M, and different subspaces will give rise to different qualitative behaviors as a function of the protocol duration, as illustrated in figure 6.

For larger systems, the number of possible measurement results in the basis $\mathcal{C}$ grows exponentially with the number of particles N. However, the number of inequivalent measurement results, whose probabilities are different, is much smaller. For instance, for $N = 12$ particles, there are $\binom{12}{6} = 924$ measurement results with total spin projection $M = 0$, among which at most 90 are inequivalent (see panels (c,f) of figure 6). This is readily exploited by grouping equivalent measurement results into a single outcome and plotting their combined probabilities $P_F^M(t)$, as we have done throughout this paper.

Outlook — Further investigation will be devoted to the robustness of our predictions with respect to: (*i*) deviations from the ideally symmetric geometries of figure 1, which may come from imperfections in the positions of the single-atom traps or from finite-temperature effects ($T = 4.5\mu$K in the recent experiment of [23]); and (*ii*) experimental uncertainties in the parameters entering equation (1) and errors in the measurement of the states of the N spins–1/2.

Acknowledgments

We acknowledge stimulating discussions with M. Brune and J.M. Raimond (LKB, Collège de France, France) and R.J. Papoular (IRAMIS, CEA Saclay, France).

Data availability statement

The data that support the findings of this study are openly available at the following URL/DOI: https://doi.org/10.5281/zenodo.22 544 497 [40].

Appendices

The three following Appendices provide additional information supporting our results. In appendix A, we summarize the various orderings used for the N-particle configurations in the basis $\mathcal{C}$. In appendix B, we identify the N-particle states of the form of equation (3) whose component with total spin projection $M = 0$ is either even or odd under the operator Y_{spin}. Finally, in appendix C, we calculate the number of inequivalent measurement results in the cases considered in the main text.

Appendix A. Orderings for the N-particle states in the basis $\mathcal{C}$

For a given particle number $N = 2n$, the Hilbert space $\mathcal{H}$ has dimension 2^N. The basis $\mathcal{C} = (|c_f\rangle)_{1\leqslant f\leqslant 2^N}$ of possible measurement results, introduced in section 2.2, is comprised of the configurations $|\mu_1, \ldots, \mu_N\rangle$, where the spin at site A_i is in the state $|\mu_i\rangle = |\uparrow_i^z\rangle$ or $|\downarrow_i^z\rangle$. They are labeled by the integer index $f = 1 + \sum_{i=1}^N (1/2 - \mu_i)\, 2^{i-1}$, where the values $\mu_i = \pm 1/2$ respectively correspond to $|\uparrow_i^z\rangle$ and $|\downarrow_i^z\rangle$. Hence, $1 \leqslant f \leqslant 2^N$, with $|c_1\rangle = |\uparrow_1^z, \ldots, \uparrow_N^z\rangle$ and $|c_{2^N}\rangle = |\downarrow_1^z, \ldots, \downarrow_N^z\rangle$.

In section 3.2, we sort the states $|c_f\rangle = |c_f^M\rangle$ in $\mathcal{C}$ in terms of their total spin projection $M = \sum_{i=1}^N \mu_i$. Hence, $S_z|c_f^M\rangle = \hbar M|c_f^M\rangle$, with the operator S_z representing the total spin projection along z. For a given M, there are $f_{\max} = \binom{N}{n+M}$ states $|c_f^M\rangle$, labeled with the integer index f such that $1 \leqslant f \leqslant f_{\max}$, ordered by increasing $\sum_{i=1}^N (1/2 - \mu_i)\, 2^{i-1}$. Thus, $|c_1^{M=0}\rangle = |\downarrow_1^z, \ldots, \downarrow_n^z; \uparrow_{n+1}^z, \ldots, \uparrow_N^z\rangle$ and $|c_{f_{\max}}^{M=0}\rangle = |\uparrow_1^z, \ldots, \uparrow_n^z; \downarrow_{n+1}^z, \ldots, \downarrow_N^z\rangle$.

Finally, in section 4.2, among the $\binom{N}{n+M}$ possible measurement results $|c_f^M\rangle$ in the basis $\mathcal{C}$ with total spin projection M, we select a subset of inequivalent states. We label them with the capital letter 'F', such that $|c_F^M\rangle = |c_f^M\rangle$, where f takes the lowest possible value among the equivalent states $|c_{f'}^M\rangle = U_\phi |c_f^M\rangle$, all in $\mathcal{C}$. The number of inequivalent measurement results $|c_F^M\rangle$ depends on the initial state $|\psi_0\rangle$. For example, for $N = 6$ particles evolving under H_{XXZ}, there are 3 inequivalent states $|c_F^{M=0}\rangle$ with total spin projection $M = 0$ if $|\psi_0\rangle = |\xi_{\boldsymbol{u}}\rangle$ or $|\eta_{\boldsymbol{u}}\rangle$, but there are 6 of them if $|\psi_0\rangle = |\chi_{\boldsymbol{u},\boldsymbol{v}}\rangle$, where the direction $\boldsymbol{v}$ is equal neither to $\boldsymbol{u}$ nor to its image under the rotation about $\boldsymbol{z}$ through angle π (see figure 4).

Appendix B. Initial states with a well-defined parity under Y^{spin}

In this section, we identify all states $|\chi\rangle = |\chi_{\boldsymbol{u},\boldsymbol{v}}\rangle$, of the form of equation (3), whose component $|\chi^{M=0}\rangle$ with total spin projection $M = 0$ is an eigenstate of the operator Y_{spin} of equation (6). Thus, we seek states $|\chi\rangle$ such that $Y_{\mathrm{spin}}|\chi^{M=0}\rangle = \epsilon|\chi^{M=0}\rangle$, where the eigenvalue $\epsilon = \pm 1$ determines the even or odd parity of $|\chi^{M=0}\rangle$ with respect to the operator Y_{spin}.

We consider the geometry involving $N = 2n$ spins. We write the single-particle state $|\uparrow^{\boldsymbol{u}}\rangle$ used for all n sites on the outer ring as $|\uparrow^{\boldsymbol{u}}\rangle = a_{\boldsymbol{u}}|\uparrow^z\rangle + b_{\boldsymbol{u}}|\downarrow^z\rangle$, where $a_{\boldsymbol{u}} = \cos(\theta_{\boldsymbol{u}}/2)\,\mathrm{e}^{-\mathrm{i}\phi_{\boldsymbol{u}}/2}$, $b_{\boldsymbol{u}} = \sin(\theta_{\boldsymbol{u}}/2)\,\mathrm{e}^{+\mathrm{i}\phi_{\boldsymbol{u}}/2}$, and the angles $(\theta_{\boldsymbol{u}}, \phi_{\boldsymbol{u}})$ are the spherical coordinates of the unit vector $\boldsymbol{u}$ on the Bloch sphere. Similarly, we write the single-particle state $|\uparrow^{\boldsymbol{v}}\rangle$ used for all n sites on the inner ring as $|\uparrow^{\boldsymbol{v}}\rangle = a_{\boldsymbol{v}}|\uparrow^z\rangle + b_{\boldsymbol{v}}|\downarrow^z\rangle$, where $a_{\boldsymbol{v}} = \cos(\theta_{\boldsymbol{v}}/2)\,\mathrm{e}^{-\mathrm{i}\phi_{\boldsymbol{v}}/2}$, $b_{\boldsymbol{v}} = \sin(\theta_{\boldsymbol{v}}/2)\,\mathrm{e}^{+\mathrm{i}\phi_{\boldsymbol{v}}/2}$, and the angles $(\theta_{\boldsymbol{v}}, \phi_{\boldsymbol{v}})$ are the spherical coordinates of the unit vector $\boldsymbol{v}$ on the Bloch sphere. No solution is found if one or more of the four complex numbers $a_{\boldsymbol{u}}$, $b_{\boldsymbol{u}}$, $a_{\boldsymbol{v}}$, $b_{\boldsymbol{v}}$ is zero, hence, we assume that they are all non-zero. The $M = 0$ component of the N-particle state $|\chi\rangle$ reads:

$$|\chi^{M=0}\rangle = \sum_{n_{O\uparrow}=0}^{n} (a_{\boldsymbol{u}}b_{\boldsymbol{v}})^{n_{O\uparrow}}\,(b_{\boldsymbol{u}}a_{\boldsymbol{v}})^{n-n_{O\uparrow}}\,|\gamma_{n_{O\uparrow}}\rangle\ , \tag{B1}$$

where the (non-normalized) N-particle state $|\gamma_{n_{O\uparrow}}\rangle$ is the sum of all states $|c_f^{M=0}\rangle$ in the basis $\mathcal{C}$ whose total spin projection is $M = 0$, and which have exactly $n_{O\uparrow}$ spins on the outer ('O') ring in the state $|\uparrow^z\rangle$. The operator Y_{spin} maps $|\chi^{M=0}\rangle$ onto:

$$Y_{\mathrm{spin}}|\chi^{M=0}\rangle = \sum_{n_{O\uparrow}=0}^{n} (-a_{\boldsymbol{u}}b_{\boldsymbol{v}})^{n-n_{O\uparrow}}\,(-b_{\boldsymbol{u}}a_{\boldsymbol{v}})^{n_{O\uparrow}}\,|\gamma_{n_{O\uparrow}}\rangle\ . \tag{B2}$$

We introduce the complex number $z = (a_{\boldsymbol{u}}b_{\boldsymbol{v}})/(b_{\boldsymbol{u}}a_{\boldsymbol{v}})$. Owing to equations (B1) and (B2), the relation $Y_{\mathrm{spin}}|\chi^{M=0}\rangle = \epsilon|\chi^{M=0}\rangle$ requires $(-z)^{n-2n_{O\uparrow}} = \epsilon$ for any integer $n_{O\uparrow}$ such that $0 \leqslant n_{O\uparrow} \leqslant n$. Hence, $z = \pm 1$. The case $z = +1$ yields the state $|\chi\rangle = |\xi_{\boldsymbol{u}}\rangle = |\chi_{\boldsymbol{u},\boldsymbol{u}}\rangle$ introduced in section 3.3, and the corresponding eigenvalue $\epsilon = (-1)^n$ depends on the parity of n. The case $z = -1$ yields the state $|\chi\rangle = |\eta_{\boldsymbol{u}}\rangle = |\chi_{\boldsymbol{u},\boldsymbol{u}'}\rangle$, where the unit vector $\boldsymbol{u}'$ on the Bloch sphere is the image of $\boldsymbol{u}$ under the rotation through angle π about the axis $\boldsymbol{z}$. The corresponding eigenvalue is $\epsilon = +1$ for all values of n.

To sum up, if n is odd, the $M = 0$ components $|\xi_{\boldsymbol{u}}^{M=0}\rangle$ and $|\eta_{\boldsymbol{u}}^{M=0}\rangle$ of the states $|\xi_{\boldsymbol{u}}\rangle$ and $|\eta_{\boldsymbol{u}}\rangle$ are respectively odd and even under the operator Y_{spin}, as illustrated in figure 4 for $n = 3$. By contrast, if n is even, both $|\xi_{\boldsymbol{u}}^{M=0}\rangle$ and $|\eta_{\boldsymbol{u}}^{M=0}\rangle$ are even with respect to Y_{spin}, and there is no state $|\chi_{\boldsymbol{u},\boldsymbol{v}}\rangle$ of the form of equation (3) whose $M = 0$ component is odd under Y_{spin}.

Appendix C. Numbers of inequivalent measurement results

C.1. Role of the spatial symmetries

In this section, we derive the number of inequivalent measurement results $|c_F^M\rangle$ for choices of the Hamiltonian (H_{H} or H_{XXZ}) and the initial state $|\psi_0\rangle$ such that the only relevant symmetries are (*i*) the spatial symmetries in the group D_{nh} and (*ii*) the conservation of the total spin projection S_z.

We consider the geometry involving $N = 2n$ particles. For a given total spin projection M, we call $\mathcal{H}^M$ the subspace of the Hilbert space $\mathcal{H}$ comprised of all N-particle states with total spin projection M. It is spanned by the $\binom{N}{n+M}$ states $|c_f^M\rangle$ in the basis $\mathcal{C}$ with total spin projection M.

The unitary operators U_ϕ acting on the Hilbert space $\mathcal{H}$, introduced in section 3.1, all commute with the total spin projection operator S_z. Hence, they leave the subspace $\mathcal{H}^M$ invariant. Thus, they make up a (reducible) representation $\mathcal{R}^M$, acting on $\mathcal{H}^M$, of the spatial symmetry group $G^{\mathrm{spatial}} = D_{nh}$. All operators U_ϕ map each state $|c_f^M\rangle$ in the basis $\mathcal{C}$ onto a state $|c_{f'}^M\rangle$, also in the basis $\mathcal{C}$ (rather than onto a linear combination of basis states). Linear representations satisfying this property are known as permutation representations [41, section 1.2].

Two possible measurement results $|c_f^M\rangle$ and $|c_{f'}^M\rangle$ are 'equivalent' if one is mapped onto the other by some symmetry operator U_ϕ, namely, $|c_{f'}^M\rangle = U_\phi|c_f^M\rangle$ (see section 4.2). Hence, the number of inequivalent measurement results is the number of different sets $\{U_\phi|c_f^M\rangle\}$, called 'orbits', obtained by applying all operators U_ϕ to each state $|c_f^M\rangle$ in $\mathcal{C}$. Owing to a known property of permutation representations

[41, section 2.3], this number is equal to the dimension of the subspace of $\mathcal{H}^M$ transforming under $\mathcal{R}^M$ according to the unit representation of D_{nh}, i.e. to the dimension $\dim(\rho_1, M)$, as stated in section 4.2.

C.2. Case of $M = 0$: role of the two-fold rotations of the N spins

We now derive the number of inequivalent measurement results $|c_F^{M=0}\rangle$ with total spin projection $M = 0$ for choices of the Hamiltonian and initial state such that, in addition to the symmetries accounted for in section C.1, the spin rotations through angle π about any horizontal axis also play a role.

The group of spin symmetries $G^{\text{spin}} = D_{\infty h}$ is comprised of the products of all rotations about the axis $\boldsymbol{z}$ through any angle, all rotations through angle π about any axis in the horizontal plane (Oxy), and inversion. The unitary operators U_g of section 3.1 make up a representation of G^{spin} acting on the Hilbert space $\mathcal{H}$. This representation is single-valued, because the considered system is comprised of an even number $N = 2n$ of spins–1/2 [27, § 99]. Inversion acts as the identity because spins are pseudovectors [35, Sec. 15.10].

The subspace $\mathcal{H}^{M=0}$ is invariant under all operators U_g. Within it, all spin rotations $C_\phi^{\boldsymbol{z}}$ about the axis $\boldsymbol{z}$ through angle ϕ act as the identity [35, section XIII.20]. Moreover, the spin rotation $C_\pi^{\boldsymbol{e}}$ through angle π about the horizontal axis with polar angle ϕ, namely, $\boldsymbol{e} = (\cos\phi, \sin\phi, 0)$, satisfies the geometric relation $C_\pi^{\boldsymbol{e}} = C_\phi^{\boldsymbol{z}} C_\pi^{\boldsymbol{x}} C_{-\phi}^{\boldsymbol{z}}$. Therefore, all spin rotations $C_\pi^{\boldsymbol{e}}$ act on $\mathcal{H}^{M=0}$ as the same operator. Hence, it is sufficient to account for a single such rotation, say $C_\pi^{\boldsymbol{y}}$. Thus, the behavior of the states in $\mathcal{H}^{M=0}$ under all spatial and spin symmetries is fully determined by the group $G_0 = D_{nh}^{\text{spatial}} \times \{1, C_\pi^{\boldsymbol{y}}\}^{\text{spin}}$, which is the direct product of the spatial symmetry group D_{nh} with a group comprised of two spin symmetries. The group G_0 is a finite subgroup of the full spin-point group G of section 3.1.

The operators U_ϕ and U_g of section 3.1 yield a reducible representation $\mathcal{R}_0$ of the group G_0 acting on the subspace $\mathcal{H}^{M=0}$. In particular, the spin rotation $C_\pi^{\boldsymbol{y}}$ acts as $Y_{\text{spin}}^{M=0}$, where:

$$Y_{\text{spin}}^{M=0} = (-1)^n F_{\text{spin}}^{M=0} \ . \tag{C1}$$

In equation (C1), $Y_{\text{spin}}^{M=0}$ and $F_{\text{spin}}^{M=0}$ are the restrictions to the subspace $\mathcal{H}^{M=0}$ of the operator Y_{spin} representing the spin rotation $C_\pi^{\boldsymbol{y}}$, and of the operator $F_{\text{spin}} = \sigma_1^x \ldots \sigma_N^x$ flipping the projection along z of each individual spin ($|\uparrow_i^z\rangle$ and $|\downarrow_i^z\rangle$ are respectively mapped onto $|\downarrow_i^z\rangle$ and $|\uparrow_i^z\rangle$).

We introduce the permutation representation $\mathcal{R}_0^+$ of G_0 acting on $\mathcal{H}^{M=0}$ defined as follows: all spatial symmetries act as in the representation $\mathcal{R}_0$, but the spin rotation $C_\pi^{y,\text{spin}}$ acts as $+F_{\text{spin}}^{M=0}$. The property of permutation representations already used in appendix C.1 above now yields the following result. The number of inequivalent measurement results $|c_F^{M=0}\rangle$ with total spin projection $M = 0$ is equal to the dimension of the subspace of $\mathcal{H}^{M=0}$ comprised of the states transforming under $\mathcal{R}_0^+$ according to the unit representation of G_0, namely, the states invariant under all spatial symmetries and under F_{spin}.

If n is even, equation (C1) shows that the representations $\mathcal{R}_0$ and $\mathcal{R}_0^+$ coincide. Then, the number of inequivalent measurement results $|c_F^{M=0}\rangle$ is $\dim(\rho_1, M = 0, \text{even}/Y_{\text{spin}})$. We have confirmed this prediction numerically for the initial states $|\xi_{\boldsymbol{x}}\rangle$ and $|\eta_{\boldsymbol{x}}\rangle$, in the cases of the geometries of figures 1(b) and (d), which respectively involve $N = 2n = 8$ and 12 atoms (for these geometries, the components $|\xi_{\boldsymbol{x}}^{M=0}\rangle$ and $|\eta_{\boldsymbol{x}}^{M=0}\rangle$ are both even under Y_{spin}: see appendix B above).

If n is odd, $F_{\text{spin}}^{M=0} = -Y_{\text{spin}}^{M=0}$, so that the number of inequivalent measurement results $|c_F^{M=0}\rangle$ is equal to $\dim(\rho_1, M = 0, \text{odd}/Y_{\text{spin}})$, which is also equal to $\dim(\rho_1, M = 0, \text{even}/Y_{\text{spin}})$ (see appendix C.3 below). This prediction is in full agreement with our numerical results, illustrated in figure 4(e) for the initial states $|\xi_{\boldsymbol{x}}\rangle$ and $|\eta_{\boldsymbol{x}}\rangle$ involving $N = 2n = 6$ atoms (geometry of figure 1(a), which are respectively eigenstates of Y_{spin} with eigenvalues -1 and $+1$.

C.3. Comparing the dimensions of the subspaces $(\rho_1, M = 0, \text{even}/Y^{\text{spin}})$ and $(\rho_1, M = 0, \text{odd}/Y^{\text{spin}})$

The dimensions $d_{\text{even}} = \dim(\rho_1, M = 0, \text{even}/F_{\text{spin}})$, $d_{\text{odd}} = \dim(\rho_1, M = 0, \text{odd}/F_{\text{spin}})$, and $d = \dim(\rho_1, M = 0)$, satisfy $d_{\text{even}} + d_{\text{odd}} = d$. We further relate the dimensions d and d_{even} by interpreting them as the numbers of orbits for two different permutation representations, both acting on the subspace $\mathcal{H}^{M=0}$ of N-particle states with total spin projection $M = 0$. The first one, $\mathcal{R}^{M=0}$, introduced in appendix C.1 above, is a representation of the spatial symmetry group D_{nh}. Its number of orbits is $d = \dim(\rho_1, M = 0)$. The second one, $\mathcal{R}_0^+$, introduced in appendix C.2, is a representation of the subgroup G_0 of the spin-point group G. Its number of orbits is $d_{\text{even}} = \dim(\rho_1, M = 0, \text{even}/F_{\text{spin}})$, the parity under F_{spin} being determined by the parity under Y_{spin} through equation (C1).

We consider the orbit Ω, under the representation $\mathcal{R}_0^+$, of the configuration $|c_{f_0}\rangle = |c_{f_0}^{M=0}\rangle$ with total spin projection $M = 0$. It is comprised of the distinct elements among $\{U_\phi |c_{f_0}\rangle\}$ and $\{F_{\rm spin} U_\phi |c_{f_0}\rangle\}$, for all spatial symmetries ϕ in D_{nh}, the operators U_ϕ being defined in section 3.1. There are two cases:

(a) If $F_{\rm spin} |c_{f_0}\rangle = U_{\phi_0} |c_{f_0}\rangle$ for some spatial symmetry ϕ_0, then all elements in Ω may be written as $U_\phi |c_{f_0}\rangle$. Thus, Ω is also an orbit under the representation $\mathcal{R}^{M=0}$.

(b) If $F_{\rm spin} |c_{f_0}\rangle \neq U_\phi |c_{f_0}\rangle$ for all spatial symmetries ϕ, Ω yields two different orbits under the representation $\mathcal{R}^{M=0}$, namely, the sets $\{U_\phi |c_{f_0}\rangle\}$ and $\{F_{\rm spin} U_\phi |c_{f_0}\rangle\}$.

We call λ_a and λ_b the numbers of orbits of $\mathcal{R}_0^+$ satisfying cases (a) and (b), respectively. Thus, $d_{\rm even}$ and d satisfy:

$$d_{\rm even} = \lambda_a + \lambda_b \quad \text{and} \quad d = \lambda_a + 2\lambda_b \ . \tag{C2}$$

Hence, the difference $d_{\rm even} - d_{\rm odd} = 2d_{\rm even} - d = \lambda_a$.

Distinction between even and odd values of n — We write $|c_{f_0}\rangle = |\mu_1, \ldots, \mu_N\rangle$ with $N = 2n$. We introduce the spin projections $M_O = \mu_1 + \ldots + \mu_n$ and $M_I = \mu_{n+1} + \ldots + \mu_N$ on the outer ('O') and inner ('I') rings, with $\mu_i = \pm 1/2$ according to whether $|\mu_i\rangle = |\uparrow_i^z\rangle$ or $|\downarrow_i^z\rangle$. For any spatial symmetry ϕ, the state $U_\phi |c_{f_0}\rangle$ has the same spin projections M_O and M_I, but the state $F_{\rm spin} |c_{f_0}\rangle$ has the spin projections $-M_O$ and $-M_I$. Therefore, case (a) requires $M_O = M_I = 0$, which is only possible if n is even. Thus, $\lambda_a = 0$ for odd values of n. To conclude, $d_{\rm even} = d_{\rm odd}$ if n is odd, and $d_{\rm even} > d_{\rm odd}$ if n is even. These results are confirmed by our explicit calculations for $n = 3$, 4, 5, and 6, summarized in table 1 of the main text.

ORCID iD

D J Papoular 0000-0001-7442-5130

References

[1] Heine V 1960 *Group Theory in Quantum Mechanics* (Pergamon)
[2] Tinkham M 1964 *Group Theory and Quantum Mechanics* (McGraw-Hill)
[3] Feynman R P, Leighton R B and Sands M 2010 *The FEynman Lectures on PHysics, Volume III* (Basic Books)
[4] Brinkman W F and Elliott R J 1966 *Proc. R. Soc. A* **294** 343
[5] Litvin D B and Opechowski W 1974 *Physica* **76** 538
[6] Xiao Z, Zhao J, Li Y, Shindou R and Song Z 2024 *Phys. Rev. X* **14** 031037
[7] Schiff H, Corticelli A, Guerreiro A, Romhányi J and McClarty P 2025 *SciPost Phys.* **18** 109
[8] Gross C and Bloch I 2017 *Science* **357** 995
[9] Browaeys A and Lahaye T 2020 *Nat. Phys.* **16** 132
[10] de Paz A, Sharma A, Chotia A, Maréchal E, Huckans J H, Pedri P, Santos L, Gorceix O, Vernac L and Laburthe-Tolra B 2013 *Phys. Rev. Lett.* **111** 185305
[11] Kaufman A M and Ni K 2021 *Nat. Phys.* **17** 1324
[12] Barredo D, de Léséleuc S, Lienhard V, Lahaye T and Browaeys A 2016 *Science* **354** 1021
[13] Barredo D, Lienhard V, de Léséleuc S, Lahaye T and Browaeys A 2018 *Nature* **561** 79
[14] Scholl P *et al* 2021 *Nature* **595** 233
[15] Ravon B, Méhaignerie P, Machu Y, Durán Hernández A, Favier M, Raimond J M, Brune M and Sayrin C 2023 *Phys. Rev. Lett.* **131** 093401
[16] Bornet G *et al* 2026 arXiv:2602.14323
[17] Nielsen M A and Chuang I L 2000 *Quantum Computation and Quantum Information* (Cambridge University Press)
[18] Yan B, Moses S A, Gadway B, Covey J P, Hazzard K R A, Rey A M, Jin D S and Ye Y 2013 *Nature* **501** 521
[19] Geier S, Thaicharoen N, Hainaut C, Franz T, Salzinger A, Tebben A, Grimshandl D, Zürn G and Weidemüller M 2021 *Science* **374** 1149
[20] Scholl P *et al* 2022 *PRX Quantum* **3** 020303
[21] Nguyen T L *et al* 2018 *Phys. Rev. X* **8** 011032
[22] Christakis L, Rosenberg J S, Raj R, Chi S, Morningstar A, Huse D A, Yan Z Z and Bakr W S 2023 *Nature* **614** 64
[23] Machu Y, Durán Hernández A, Creutzer G, Young A A, Raimond J-M, Brune M and Sayrin C 2026 *Phys. Rev. X* **16** 021040
[24] Ebadi S *et al* 2021 *Nature* **595** 227
[25] Messiah A 1961 *Quantum Mechanics, Volume I* (North Holland, Amsterdam)
[26] Cotton F A 1990 *Chemical Applications of Group Theory* 3rd edn (Wiley)
[27] Landau L D and Lifshitz E M 1977 *Quantum Mechanics, non-Relativistic Theory* 3rd edn (Butterworth-Heinemann, Oxford)
[28] Cohen-Tannoudji C, Diu B and Laloë F 2020 *Quantum Mechanics, Volume I* 2nd edn (Wiley)
[29] Musolino S, Albert M, Minguzzi A and Vignolo P 2024 *Phys. Rev. Lett.* **133** 183402
[30] Antonić L, Kafri Y, Podolsky D and Turner A M 2025 *Phys. Rev. B* **111** 224305

[31] Eberly J H, Narozhny N B and Sanchez-Mondragon J J 1980 *Phys. Rev. Lett.* **44** 1323
[32] Rempe G, Walther H and Klein N 1987 *Phys. Rev. Lett.* **58** 353
[33] Greiner M, Mandel O, Hänsch T W and Bloch I 2002 *Nature* **419** 51
[34] Nogrette F, Labuhn H, Ravets S, Barredo D, Béguin L, Vernier A, Lahaye T and Browaeys A 2014 *Phys. Rev. X* **4** 021034
[35] Messiah A 1962 *Quantum Mechanics, Volume II* (North Holland, Amsterdam)
[36] Ashcroft N W and Mermin N D 1976 *Solid State Physics* (Saunders)
[37] Harris C R *et al* 2020 *Nature* **585** 357
[38] Virtanen P *et al* 2020 *Nat. Methods* **17** 261
[39] Brigham E O 1988 *The Fast Fourier Transform and its Applications* (Prentice Hall)
[40] Papoular D J 2026 Dataset for the article entitled "Measured dynamics of an XXZ quantum simulator in a highly symmetrical double-ringed geometry" *Zenodo* https://doi.org/10.5281/zenodo.22544497
[41] Serre J P 1977 *Linear Representations of Finite Groups* (Springer)